

SEARCHES FOR CONTINUOUS GRAVITATIONAL WAVES FROM NINE YOUNG SUPERNOVA REMNANTS

J. AASI¹, B. P. ABBOTT¹, R. ABBOTT¹, T. ABBOTT², M. R. ABERNATHY¹, F. ACERNESE^{3,4}, K. ACKLEY⁵, C. ADAMS⁶,
T. ADAMS^{7,8}, P. ADDESSO⁹, R. X. ADHIKARI¹, V. ADYA¹⁰, C. AFFELDT¹⁰, M. AGATHOS¹¹, K. AGATSUMA¹¹,
N. AGGARWAL¹², O. D. AGUIAR¹³, A. AIN¹⁴, P. AJITH¹⁵, A. ALEMIC¹⁶, B. ALLEN^{17,18}, A. ALLOCCA^{19,20}, D. AMARIUTEI⁵,
S. B. ANDERSON¹, W. G. ANDERSON¹⁸, K. ARAI¹, M. C. ARAYA¹, C. ARCENEUX²¹, J. S. AREEDA²², S. AST²³,
S. M. ASTON⁶, P. ASTONE²⁴, P. AUFMUTH²³, C. AULBERT¹⁷, B. E. AYLOTT²⁵, S. BABAK²⁶, P. T. BAKER²⁷,
F. BALDACCINI^{28,29}, G. BALLARDIN³⁰, S. W. BALLMER¹⁶, J. C. BARAYOGA¹, M. BARBET⁵, S. BARCLAY³¹, B. C. BARISH¹,
D. BARKER³², F. BARONE^{3,4}, B. BARR³¹, L. BARSOTTI¹², M. BARSUGLIA³³, J. BARTLETT³², M. A. BARTON³², I. BARTOS³⁴,
R. BASSIRI³⁵, A. BASTI^{36,20}, J. C. BATCH³², T. S. BAUER¹¹, C. BAUNE¹⁰, V. BAVIGADDA³⁰, B. BEHNKE²⁶, M. BEJGER³⁷,
C. BELCZYNSKI³⁸, A. S. BELL³¹, C. BELL³¹, M. BENACQUISTA³⁹, J. BERGMAN³², G. BERGMANN¹⁰, C. P. L. BERRY²⁵,
D. BERSANETTI^{40,41}, A. BERTOLINI¹¹, J. BETZWIESER⁶, S. BHAGWAT¹⁶, R. BHANDARE⁴², I. A. BILENKO⁴³,
G. BILLINGSLEY¹, J. BIRCH⁶, S. BISCANS¹², M. BITOSI^{30,20}, C. BIWER¹⁶, M. A. BIZOUARD⁴⁴, J. K. BLACKBURN¹,
L. BLACKBURN⁴⁵, C. D. BLAIR⁴⁶, D. BLAIR⁴⁶, S. BLOEMEN^{11,47}, O. BOCK¹⁷, T. P. BODIYA¹², M. BOER⁴⁸, G. BOGAERT⁴⁸,
P. BOJTOS⁴⁹, C. BOND²⁵, F. BONDU⁵⁰, L. BONELLI^{36,20}, R. BONNAND⁸, R. BORK¹, M. BORN¹⁰, V. BOSCHI²⁰,
SUKANTA BOSE^{14,51}, C. BRADASCHIA²⁰, P. R. BRADY¹⁸, V. B. BRAGINSKY⁴³, M. BRANCHESI^{52,53}, J. E. BRAU⁵⁴,
T. BRIANT⁵⁵, D. O. BRIDGES⁶, A. BRILLET⁴⁸, M. BRINKMANN¹⁰, V. BRISSON⁴⁴, A. F. BROOKS¹, D. A. BROWN¹⁶,
D. D. BROWN²⁵, N. M. BROWN¹², S. BUCHMAN³⁵, A. BUIKEMA¹², T. BULIK³⁸, H. J. BULTEN^{56,11}, A. BUONANNO⁵⁷,
D. BUSKULIC⁸, C. BUY³³, L. CADONATI⁵⁸, G. CAGNOLI⁵⁹, J. CALDERÓN BUSTILLO⁶⁰, E. CALLONI^{61,4}, J. B. CAMP⁴⁵,
K. C. CANNON⁶², J. CAO⁶³, C. D. CAPANO⁵⁷, F. CARBOGNANI³⁰, S. CARIDE⁶⁴, S. CAUDILL¹⁸, M. CAVAGLIA²¹,
F. CAVALIER⁴⁴, R. CAVALIERI³⁰, G. CELLA²⁰, C. CEPEDA¹, E. CESARINI⁶⁵, R. CHAKRABORTY¹, T. CHALERMSONGSAK¹,
S. J. CHAMBERLIN¹⁸, S. CHAO⁶⁶, P. CHARLTON⁶⁷, E. CHASSANDE-MOTTIN³³, Y. CHEN⁶⁸, A. CHINCARINI⁴¹, A. CHIUMMO³⁰,
H. S. CHO⁶⁹, M. CHO⁵⁷, J. H. CHOW⁷⁰, N. CHRISTENSEN⁷¹, Q. CHU⁴⁶, S. CHUA⁵⁵, S. CHUNG⁴⁶, G. CIANI⁵, F. CLARA³²,
J. A. CLARK⁵⁸, F. CLEVA⁴⁸, E. COCCIA^{72,73}, P.-F. COHADON⁵, A. COLLA^{74,24}, C. COLLETTE⁷⁵, M. COLOMBINI²⁹,
L. COMINSKY⁷⁶, M. CONSTANCIO, JR.¹³, A. CONTE^{74,24}, D. COOK³², T. R. CORBITT², N. CORNISH²⁷, A. CORSI⁷⁷,
C. A. COSTA¹³, M. W. COUGHLIN⁷¹, J.-P. COULON⁴⁸, S. COUNTRYMAN³⁴, P. COUVARES¹⁶, D. M. COWARD⁴⁶,
M. J. COWART⁶, D. C. COYNE¹, R. COYNE⁷⁷, K. CRAIG³¹, J. D. E. CREIGHTON¹⁸, T. D. CREIGHTON³⁹, J. CRIPE²,
S. G. CROWDER⁷⁸, A. CUMMING³¹, L. CUNNINGHAM³¹, E. CUOCO³⁰, C. CUTLER⁶⁸, K. DAHL¹⁰, T. DAL CANTON¹⁷,
M. DAMJANIC¹⁰, S. L. DANILISHIN⁴⁶, S. D'ANTONIO⁶⁵, K. DANZMANN^{23,10}, L. DARTEZ³⁹, V. DATILLO³⁰, I. DAVE⁴²,
H. DAVELOZA³⁹, M. DAVIER⁴⁴, G. S. DAVIES³¹, E. J. DAW⁷⁹, R. DAY³⁰, D. DEBRA³⁵, G. DEBRECZENI⁸⁰, J. DEGALLAIX⁵⁹,
M. DE LAURENTIS^{61,4}, S. DELÉGLISE⁵⁵, W. DEL POZZO²⁵, T. DENKER¹⁰, T. DENT¹⁷, H. DERELI⁴⁸, V. DERGACHEV¹,
R. DE ROSA^{61,4}, R. T. DEROSA², R. DESALVO⁹, S. DHURANDHAR¹⁴, M. DÍAZ³⁹, L. DI FIORE⁴, A. DI LIETO^{36,20},
I. DI PALMA²⁶, A. DI VIRGILIO²⁰, G. DOJCINOSKI⁸¹, V. DOLIQUE⁵⁹, E. DOMINGUEZ⁸², F. DONOVAN¹², K. L. DOOLEY¹⁰,
S. DORAVARI⁶, R. DOUGLAS³¹, T. P. DOWNES¹⁸, M. DRAGO^{83,84}, J. C. DRIGGERS¹, Z. DU⁶³, M. DUCROT⁸, S. DWYER³²,
T. EBERLE¹⁰, T. EDO⁷⁹, M. EDWARDS⁷, M. EDWARDS⁷¹, A. EFFLER³², H.-B. EGGENSTEIN¹⁷, P. EHRENS¹, J. EICHWOLZ⁵,
S. S. EIKENBERRY⁵, R. ESSICK¹², T. ETZEL¹, M. EVANS¹², T. EVANS⁶, M. FACTOUROVICH³⁴, V. FAFONE^{72,65},
S. FAIRHURST⁷, X. FAN³¹, Q. FANG⁴⁶, S. FARINON⁴¹, B. FARR⁸⁵, W. M. FARR²⁵, M. FAVATA⁸¹, M. FAYS⁷, H. FEHRMANN¹⁷,
M. M. FEJER³⁵, D. FELDBAUM^{5,6}, I. FERRANTE^{36,20}, E. C. FERREIRA¹³, F. FERRINI³⁰, F. FIDECARO^{36,20}, I. FIORI³⁰,
R. P. FISHER¹⁶, R. FLAMINIO⁵⁹, J.-D. FOURNIER⁴⁸, S. FRANCO⁴⁴, S. FRASCA^{74,24}, F. FRASCONI²⁰, Z. FREI⁴⁹, A. FREISE²⁵,
R. FREY⁵⁴, T. T. FRICKE¹⁰, P. FRITSCHEL¹², V. V. FROLOV⁶, S. FUENTES-TAPIA³⁹, P. FULDA⁵, M. FYFFE⁶, J. R. GAIR⁸⁶,
L. GAMMAITONI^{28,29}, S. GAONKAR¹⁴, F. GARUFI^{61,4}, A. GATTO³³, N. GEHRELS⁴⁵, G. GEMME⁴¹, B. GENDRE⁴⁸, E. GENIN³⁰,
A. GENNAI²⁰, L. Á. GERGELY⁸⁷, S. GHOSH^{11,47}, J. A. GIAIME^{6,2}, K. D. GIARDINA⁶, A. GIAZOTTO²⁰, J. GLEASON⁵,
E. GOETZ¹⁷, R. GOETZ⁵, L. GONDAN⁴⁹, G. GONZÁLEZ², N. GORDON³¹, M. L. GORODETSKY⁴³, S. GOSSAN⁶⁸, S. GOSSLER¹⁰,
R. GOUATY⁸, C. GRÄF³¹, P. B. GRAFF⁴⁵, M. GRANATA⁵⁹, A. GRANT³¹, S. GRAS¹², C. GRAY³², R. J. S. GREENHALGH⁸⁸,
A. M. GRETARSSON⁸⁹, P. GROOT⁴⁷, H. GROTE¹⁰, S. GRUNEWALD²⁶, G. M. GUIDI^{52,53}, C. J. GUIDO⁶, X. GUO⁶³,
K. GUSHWA¹, E. K. GUSTAFSON¹, R. GUSTAFSON⁶⁴, J. HACKER²², E. D. HALL¹, G. HAMMOND³¹, M. HANKE¹⁰, J. HANKS³²,
C. HANNA⁹⁰, M. D. HANNAM⁷, J. HANSON⁶, T. HARDWICK^{54,2}, J. HARMS⁵³, G. M. HARRY⁹¹, I. W. HARRY²⁶, M. HART³¹,
M. T. HARTMAN⁵, C.-J. HASTER²⁵, K. HAUGHIAN³¹, A. HEIDMANN⁵⁵, M. HEINTZE^{5,6}, G. HEINZEL¹⁰, H. HEITMANN⁴⁸,
P. HELLO⁴⁴, G. HEMMING³⁰, M. HENDRY³¹, I. S. HENG³¹, A. W. HEPTONSTALL¹, M. HEURS¹⁰, M. HEWITSON¹⁰, S. HILD³¹,
D. HOAK⁵⁸, K. A. HODGE¹, D. HOFMAN⁵⁹, S. E. HOLLITT⁹², K. HOLT⁶, P. HOPKINS⁷, D. J. HOSKEN⁹², J. HOUGH³¹,
E. HOUSTON³¹, E. J. HOWELL⁴⁶, Y. M. HU³¹, E. HUERTA⁹³, B. HUGHEY⁸⁹, S. HUSA⁶⁰, S. H. HUTTNER³¹, M. HUYNH¹⁸,
T. HUYNH-DINH⁶, A. IDRISY⁹⁰, N. INDIK¹⁷, D. R. INGRAM³², R. INTA⁹⁰, G. ISLAS²², J. C. ISLER¹⁶, T. ISOGAI¹²,
B. R. IYER⁹⁴, K. IZUMI³², M. JACOBSON¹, H. JANG⁹⁵, P. JARANOWSKI⁹⁶, S. JAWAHAR⁹⁷, Y. JI⁶³, F. JIMÉNEZ-FORTEZA⁶⁰,
W. W. JOHNSON², D. I. JONES⁹⁸, R. JONES³¹, R. J. G. JONKER¹¹, L. JU⁴⁶, HARIS K⁹⁹, V. KALOGERA⁸⁵, S. KANDHASAMY²¹,
G. KANG⁹⁵, J. B. KANNER¹, M. KASPRZACK^{44,30}, E. KATSAVOUNIDIS¹², W. KATZMAN⁶, H. KAUFER²³, S. KAUFER²³,
T. KAUR⁴⁶, K. KAWABE³², F. KAWAZOE¹⁰, F. KÉPÉLIAN⁴⁸, G. M. KEISER³⁵, D. KEITEL¹⁷, D. B. KELLEY¹⁶, W. KELLS¹,
D. G. KEPPEL¹⁷, J. S. KEY³⁹, A. KHALAIDOVSKI¹⁰, F. Y. KHALILI⁴³, E. A. KHAZANOV¹⁰⁰, C. KIM^{101,95}, K. KIM¹⁰²,
N. G. KIM⁹⁵, N. KIM³⁵, Y.-M. KIM⁶⁹, E. J. KING⁹², P. J. KING³², D. L. KINZEL⁶, J. S. KISSEL³², S. KLIMENKO⁵,
J. KLINE¹⁸, S. KOEHLLENBECK¹⁰, K. KOKEYAMA², V. KONDRASHOV¹¹, M. KOROBKO¹⁰, W. Z. KORTH¹, I. KOWALSKA³⁸,
D. B. KOZAK¹, V. KRINGEL¹⁰, B. KRISHNAN¹⁷, A. KRÓLAK^{103,104}, C. KRUEGER²³, G. KUEHN¹⁰, A. KUMAR¹⁰⁵,
P. KUMAR¹⁶, L. KUO⁶⁶, A. KUTYNYA¹⁰³, M. L. LANDRY³², B. LANTZ³⁵, S. LARSON⁸⁵, P. D. LASKY¹⁰⁶, A. LAZZARINI¹,
C. LAZZARO¹⁰⁷, C. LAZZARO⁵⁸, J. LE⁸⁵, P. LEACI²⁶, S. LEAVEY³¹, E. LEBIGOT³³, E. O. LEBIGOT⁶³, C. H. LEE⁶⁹,
H. K. LEE¹⁰², H. M. LEE¹⁰¹, M. LEONARDI^{83,84}, J. R. LEONG¹⁰, N. LEROY⁴⁴, N. LETENDRE⁸, Y. LEVIN¹⁰⁸, B. LEVINE³²,
J. LEWIS²², T. G. F. LI¹, K. LIBBRECHT¹, A. LIBSON¹², A. C. LIN³⁵, T. B. LITTENBERG⁸⁵, N. A. LOCKERBIE⁹⁷,
V. LOCKETT²², J. LOGUE³¹, A. L. LOMBARDI⁵⁸, M. LORENZINI⁷³, V. LORIETTE¹⁰⁹, M. LORMAND⁶, G. LOSURDO⁵³,
J. LOUGH¹⁷, M. J. LUBINSKI³², H. LÜCK^{23,10}, A. P. LUNDGREN¹⁷, R. LYNCH¹², Y. MA⁴⁶, J. MACARTHUR³¹,

T. MACDONALD³⁵, B. MACHENSCHALK¹⁷, M. MACINNIS¹², D. M. MACLEOD², F. MAGAÑA-SANDOVAL¹⁶, R. MAGEE⁵¹, M. MAGESWARAN¹, C. MAGLIONE⁸², K. MAILAND¹, E. MAJORANA²⁴, I. MAKSIMOVIC¹⁰⁹, V. MALVEZZI^{72,65}, N. MAN⁴⁸, I. MANDEL²⁵, V. MANDIC⁷⁸, V. MANGANO³¹, V. MANGANO^{74,24}, G. L. MANSSELL⁷⁰, M. MANTOVANI^{30,20}, F. MARCHESONI^{110,29}, F. MARION⁸, S. MÁRKA³⁴, Z. MÁRKA³⁴, A. MARKOSYAN³⁵, E. MAROS¹², F. MARTELLI^{52,53}, L. MARTELLINI⁴⁸, I. W. MARTIN³¹, R. M. MARTIN⁵, D. MARTYNOV¹, J. N. MARX¹, K. MASON¹², A. MASSEROT⁸, T. J. MASSINGER¹⁶, F. MATICHARD¹², L. MATONE³⁴, N. MAVALVALA¹², N. MAZUMDER⁹⁹, G. MAZZOLO¹⁷, R. MCCARTHY³², D. E. MCCLELLAND⁷⁰, S. MCCORMICK⁶, S. C. MCGUIRE¹¹¹, G. MCINTYRE¹, J. MCIVER⁵⁸, K. MCLIN⁷⁶, S. MCWILLIAMS⁹³, D. MEACHER⁴⁸, G. D. MEADORS⁶⁴, J. MEIDAM¹¹, M. MEINDERS²³, A. MELATOS¹⁰⁶, G. MENDELL³², R. A. MERCER¹⁸, S. MESHKOV¹, C. MESSENGER³¹, P. M. MEYERS⁷⁸, F. MEZZANI^{24,74}, H. MIAO²⁵, C. MICHEL⁵⁹, H. MIDDLETON²⁵, E. E. MIKHAILOV¹¹², L. MILANO^{61,4}, A. MILLER¹¹³, J. MILLER¹², M. MILLHOUSE²⁷, Y. MINENKOV⁶⁵, J. MING²⁶, S. MIRSHKARI¹¹⁴, C. MISHRA¹⁵, S. MITRA¹⁴, V. P. MITROFANOV⁴³, G. MITSELMAKHER⁵, R. MITTLEMAN¹², B. MOE¹⁸, A. MOGGI²⁰, M. MOHAN³⁰, S. D. MOHANTY³⁹, S. R. P. MOHAPATRA¹², B. MOORE⁸¹, D. MORARU³², G. MORENO³², S. R. MORRIS³⁹, K. MOSSAVI¹⁰, B. MOURS⁸, C. M. MOW-LOWRY¹⁰, C. L. MUELLER⁵, G. MUELLER⁵, S. MUKHERJEE³⁹, A. MULLAVEY⁶, J. MUNCH⁹², D. MURPHY³⁴, P. G. MURRAY³¹, A. MYTIDIS⁵, M. F. NAGY⁸⁰, I. NARDECCHIA^{72,65}, T. NASH¹, L. NATICCHIONI⁷⁰, R. K. NAYAK¹¹⁵, V. NECULA⁵, K. NEDKOVA⁵⁸, G. NELEMANS^{11,47}, I. NERI^{28,29}, M. NERI^{40,41}, G. NEWTON³¹, T. NGUYEN⁷⁰, A. B. NIELSEN¹⁷, S. NISSANKE⁶⁸, A. H. NITZ¹⁶, F. NOCERA³⁰, D. NOLTING⁶, M. E. N. NORMANDIN³⁹, L. K. NUTTALL¹⁸, E. OCHSNER¹⁸, J. O'DELL⁸⁸, E. OELKER¹², G. H. OGIN¹¹⁶, J. J. OH¹¹⁷, S. H. OH¹¹⁷, F. OHME⁷, P. OPPERMANN¹⁰, R. ORAM⁶, B. O'REILLY⁶, W. ORTEGA⁸², R. O'SHAUGHNESSY¹¹⁸, C. OSTHELDER¹, C. D. OTT⁶⁸, D. J. OTTAWAY⁹², R. S. OTTENS⁵, H. OVERMIER⁶, B. J. OWEN⁹⁰, C. PADILLA²², A. PAI⁹⁹, S. PAI⁴², O. PALASHOV¹⁰⁰, C. PALOMBA²⁴, A. PAL-SINGH¹⁰, H. PAN⁶⁶, C. PANKOW¹⁸, F. PANNARALE⁷, B. C. PANT⁴², F. PAOLETTI^{30,20}, M. A. PAPA^{18,26}, H. PARIS³⁵, A. PASQUALETTI³⁰, R. PASSAQUETI^{36,20}, D. PASSUELLO²⁰, Z. PATRICK³⁵, M. PEDRAZA¹, L. PEKOWSKY¹⁶, A. PELE³², S. PENN¹¹⁹, A. PERRECA¹⁶, M. PHELPS¹, M. PICHOT⁴⁸, F. PIERGIOVANNI^{52,53}, V. PIERRO⁹, G. PILLANT³⁰, L. PINARD⁵⁹, I. M. PINTO⁹, M. PITKIN³¹, J. POELD¹⁰, R. POGGIANI^{36,20}, A. POST¹⁷, A. POTEOMKIN¹⁰⁰, J. POWELL³¹, J. PRASAD¹⁴, V. PREDOI⁷, S. PREMACHANDRA¹⁰⁸, T. PRESTEGARD⁷⁸, L. R. PRICE¹, M. PRIJATELJ³⁰, M. PRINCIPE⁹, S. PRIVITERA¹, R. PRIX¹⁷, G. A. PRODI^{83,84}, L. PROKHOROV⁴³, O. PUNCKEN³⁹, M. PUNTURO²⁹, P. PUPPO²⁴, M. PÜRRE⁷, J. QIN⁴⁶, V. QUETSCHKE³⁹, E. QUINTERO¹, G. QUIROGA⁸², R. QUITZOW-JAMES⁵⁴, F. J. RAAB³², D. S. RABELING^{70,56,11}, I. RÁCZ⁸⁰, H. RADKINS³², P. RAFFAI⁴⁹, S. RAJA⁴², G. RAJALAKSHMI¹²⁰, M. RAKHMANOV³⁹, K. RAMIREZ³⁹, P. RAPAGNANI^{74,24}, V. RAYMOND¹, M. RAZZANO^{36,20}, V. RE^{72,65}, C. M. REED³², T. REGIMBAU⁴⁸, L. REI⁴¹, S. REID¹²¹, D. H. REITZE^{1,5}, O. REULA⁸², F. RICCI^{74,24}, K. RILES⁶⁴, N. A. ROBERTSON^{1,31}, R. ROBBIE³¹, F. ROBINET⁴⁴, A. ROCCHI⁶⁵, L. ROLLAND⁸, J. G. ROLLINS¹, V. ROMA⁵⁴, R. ROMANO^{3,4}, G. ROMANOV¹¹², J. H. ROMIE⁶, D. ROSIŃSKA^{122,37}, S. ROWAN³¹, A. RÜDIGER¹⁰, P. RUGGI³⁰, K. RYAN³², S. SACHDEV¹, T. SADECKI³², L. SADEGHIAN¹⁸, M. SALEEM⁹⁹, F. SALEMI¹⁷, L. SAMMUT¹⁰⁶, V. SANDBERG³², J. R. SANDERS⁶⁴, V. SANNIBALE¹, I. SANTIAGO-PRieto³¹, B. SASSOLAS⁵⁹, B. S. SATHYAPRAKASH⁷, P. R. SAULSON¹⁶, R. SAVAGE³², A. SAWADSKY²³, J. SCHEUER⁸⁵, R. SCHILLING¹⁰, P. SCHMIDT^{7,1}, R. SCHNABEL^{10,123}, R. M. S. SCHOFIELD⁵⁴, E. SCHREIBER¹⁰, D. SCHUETTE¹⁰, B. F. SCHUTZ^{7,26}, J. SCOTT³¹, S. M. SCOTT⁷⁰, D. SELLERS⁶, A. S. SENGUPTA¹²⁴, D. SENTENAC³⁰, V. SEQUINO^{72,65}, A. SERGEEV¹⁰⁰, G. SERNA²², A. SEVIGNY³², D. A. SHADDOCK⁷⁰, S. SHAH^{11,47}, M. S. SHAHRIAR⁸⁵, M. SHALTEV¹⁷, Z. SHAO¹, B. SHAPIRO³⁵, P. SHAWHAN⁵⁷, D. H. SHOEMAKER¹², T. L. SIDERY²⁵, K. SIELLEZ⁴⁸, X. SIEMENS¹⁸, D. SIGG³², A. D. SILVA¹³, D. SIMAKOV¹⁰, A. SINGER¹, L. SINGER¹, R. SINGH², A. M. SINTES⁶⁰, B. J. J. SLAGMOLEN⁷⁰, J. R. SMITH²², M. R. SMITH¹, R. J. E. SMITH¹, N. D. SMITH-LEFEBVRE¹, E. J. SON¹¹⁷, B. SORAZU³¹, T. SOURADEEP¹⁴, A. STALEY³⁴, J. STEBBINS³⁵, M. STEINKE¹⁰, J. STEINLECHNER³¹, S. STEINLECHNER³¹, D. STEINMEYER¹⁰, B. C. STEPHENS¹⁸, S. STEPLEWSKI⁵¹, S. STEVENSON²⁵, R. STONE³⁹, K. A. STRAIN³¹, N. STRANIERO⁵⁹, S. STRIGIN⁴³, R. STURANI¹¹⁴, A. L. STUVER⁶, T. Z. SUMMERSCALES¹²⁵, P. J. SUTTON⁷, B. SWINKELS³⁰, M. SZCZEPANCIK⁸⁹, G. SZEIFERT⁴⁹, M. TACCA³³, D. TALUKDER⁵⁴, D. B. TANNER⁵, M. TÁPAI⁸⁷, S. P. TARABRIN¹⁰, A. TARACCHINI⁵⁷, R. TAYLOR¹, G. TELLEZ³⁹, T. THEEG¹⁰, M. P. THIRUGNANASAMBANDAM¹, M. THOMAS⁶, P. THOMAS³², K. A. THORNE⁶, K. S. THORNE⁶⁸, E. THRANE^{1,108}, V. TIWARI⁵, C. TOMLINSON⁷⁹, M. TONELLI^{36,20}, C. V. TORRES³⁹, C. I. TORRIE^{1,31}, F. TRAVASSO^{28,29}, G. TRAYLOR⁶, M. TSE¹², D. TSHILUMBA⁷⁵, D. UGOLINI¹²⁶, C. S. UNNIKRISHNAN¹²⁰, A. L. URBAN¹⁸, S. A. USMAN¹⁶, H. VAHLBRUCH²³, G. VAJENTE¹, G. VAJENTE^{36,20}, G. VALDES³⁹, M. VALLISNERI⁶⁸, N. VAN BAKEL¹¹, M. VAN BEUZekom¹¹, J. F. J. VAN DEN BRAND^{56,11}, C. VAN DEN BROECK¹¹, M. V. VAN DER SLUYS^{11,47}, J. VAN HELMINGEN¹¹, A. A. VAN VEGGEL³¹, S. VASS¹, M. VASÚTH⁸⁰, R. VAULIN¹², A. VECCHIO²⁵, G. VEDOVATO¹⁰⁷, J. VEITCH²⁵, J. VEITCH¹¹, P. J. VEITCH⁹², K. VENKATESWARA¹²⁷, D. VERKINDT⁸, F. VETRANO^{52,53}, A. VICERÉ^{52,53}, R. VINCENT-FINLEY¹¹¹, J.-Y. VINET⁴⁸, S. VITALE¹², T. VO³², H. VOCCA^{28,29}, C. VORVICK³², W. D. VOUSDEN²⁵, S. P. VYATCHANIN⁴³, A. R. WADE⁷⁰, L. WADE¹⁸, M. WADE¹⁸, M. WALKER², L. WALLACE¹, S. WALSH¹⁸, H. WANG²⁵, M. WANG²⁵, X. WANG⁶³, R. L. WARD⁷⁰, J. WARNER³², M. WAS¹⁰, B. WEAVER³², L.-W. WEI⁴⁸, M. WEINERT¹⁰, A. J. WEINSTEIN¹, R. WEISS¹², T. WELBORN⁶, L. WEN⁴⁶, P. WESSELS¹⁰, T. WESTPHAL¹⁰, K. WETTE¹⁷, J. T. WHELAN^{118,17}, D. J. WHITE⁷⁹, B. F. WHITING⁵, C. WILKINSON³², L. WILLIAMS⁵, R. WILLIAMS¹, A. R. WILLIAMSON⁷, J. L. WILLIS¹¹³, B. WILLEKE^{23,10}, M. WIMMER¹⁰, W. WINKLER¹⁰, C. C. WIPF¹², H. WITTEL¹⁰, G. WOAN³¹, J. WORDEN³², S. XIE⁷⁵, J. YABLON⁸⁵, I. YAKUSHIN⁶, W. YAM¹², H. YAMAMOTO¹, C. C. YANCEY⁵⁷, Q. YANG⁶³, M. YVERT⁸, A. ZADROŻNY¹⁰³, M. ZANOLIN⁸⁹, J.-P. ZENDRI¹⁰⁷, FAN ZHANG^{12,63}, L. ZHANG¹, M. ZHANG¹¹², Y. ZHANG¹¹⁸, C. ZHAO⁴⁶, M. ZHOU⁸⁵, X. J. ZHU⁴⁶, M. E. ZUCKER¹², S. ZURAW⁵⁸, AND J. ZWEIZIG¹

¹LIGO, California Institute of Technology, Pasadena, CA 91125, USA

²Louisiana State University, Baton Rouge, LA 70803, USA

³Università di Salerno, Fisciano, I-84084 Salerno, Italy

⁴INFN, Sezione di Napoli, Complesso Universitario di Monte Sant'Angelo, I-80126 Napoli, Italy

⁵University of Florida, Gainesville, FL 32611, USA

⁶LIGO Livingston Observatory, Livingston, LA 70754, USA

⁷Cardiff University, Cardiff, CF24 3AA, United Kingdom

⁸Laboratoire d'Annecy-le-Vieux de Physique des Particules (LAPP), Université de Savoie, CNRS/IN2P3, F-74941 Annecy-le-Vieux, France

⁹University of Sannio at Benevento, I-82100 Benevento, Italy and INFN, Sezione di Napoli, I-80100 Napoli, Italy

¹⁰Experimental Group, Albert-Einstein-Institut, Max-Planck-Institut für Gravitationsphysik, D-30167 Hannover, Germany

¹¹Nikhef, Science Park, 1098 XG Amsterdam, The Netherlands

- ¹²LIGO, Massachusetts Institute of Technology, Cambridge, MA 02139, USA
- ¹³Instituto Nacional de Pesquisas Espaciais, 12227-010 São José dos Campos, SP, Brazil
- ¹⁴Inter-University Centre for Astronomy and Astrophysics, Pune 411007, India
- ¹⁵International Centre for Theoretical Sciences, Tata Institute of Fundamental Research, Bangalore 560012, India
- ¹⁶Syracuse University, Syracuse, NY 13244, USA
- ¹⁷Data Analysis Group, Albert-Einstein-Institut, Max-Planck-Institut für Gravitationsphysik, D-30167 Hannover, Germany
- ¹⁸University of Wisconsin–Milwaukee, Milwaukee, WI 53201, USA
- ¹⁹Università di Siena, I-53100 Siena, Italy
- ²⁰INFN, Sezione di Pisa, I-56127 Pisa, Italy
- ²¹The University of Mississippi, University, MS 38677, USA
- ²²California State University Fullerton, Fullerton, CA 92831, USA
- ²³Leibniz Universität Hannover, D-30167 Hannover, Germany
- ²⁴INFN, Sezione di Roma, I-00185 Roma, Italy
- ²⁵University of Birmingham, Birmingham, B15 2TT, United Kingdom
- ²⁶Albert-Einstein-Institut, Max-Planck-Institut für Gravitationsphysik, D-14476 Golm, Germany
- ²⁷Montana State University, Bozeman, MT 59717, USA
- ²⁸Università di Perugia, I-06123 Perugia, Italy
- ²⁹INFN, Sezione di Perugia, I-06123 Perugia, Italy
- ³⁰European Gravitational Observatory (EGO), I-56021 Cascina, Pisa, Italy
- ³¹SUPA, University of Glasgow, Glasgow, G12 8QQ, United Kingdom
- ³²LIGO Hanford Observatory, Richland, WA 99352, USA
- ³³APC, AstroParticule et Cosmologie, Université Paris Diderot, CNRS/IN2P3, CEA/Irfu, Observatoire de Paris, Sorbonne Paris Cité, 10, rue Alice Domon et Léonie Duquet, F-75205 Paris Cedex 13, France
- ³⁴Columbia University, New York, NY 10027, USA
- ³⁵Stanford University, Stanford, CA 94305, USA
- ³⁶Università di Pisa, I-56127 Pisa, Italy
- ³⁷CAMK-PAN, 00-716 Warsaw, Poland
- ³⁸Astronomical Observatory Warsaw University, 00-478 Warsaw, Poland
- ³⁹The University of Texas at Brownsville, Brownsville, TX 78520, USA
- ⁴⁰Università degli Studi di Genova, I-16146 Genova, Italy
- ⁴¹INFN, Sezione di Genova, I-16146 Genova, Italy
- ⁴²RRCAT, Indore MP 452013, India
- ⁴³Faculty of Physics, Lomonosov Moscow State University, Moscow 119991, Russia
- ⁴⁴LAL, Université Paris-Sud, IN2P3/CNRS, F-91898 Orsay, France
- ⁴⁵NASA/Goddard Space Flight Center, Greenbelt, MD 20771, USA
- ⁴⁶University of Western Australia, Crawley, WA 6009, Australia
- ⁴⁷Department of Astrophysics/IMAPP, Radboud University Nijmegen, P.O. Box 9010, 6500 GL Nijmegen, The Netherlands
- ⁴⁸ARTEMIS, Université Nice-Sophia-Antipolis, CNRS and Observatoire de la Côte d'Azur, F-06304 Nice, France
- ⁴⁹MTA Eötvös University, 'Lendület' Astrophysics Research Group, Budapest 1117, Hungary
- ⁵⁰Institut de Physique de Rennes, CNRS, Université de Rennes 1, F-35042 Rennes, France
- ⁵¹Washington State University, Pullman, WA 99164, USA
- ⁵²Università degli Studi di Urbino 'Carlo Bo', I-61029 Urbino, Italy
- ⁵³INFN, Sezione di Firenze, I-50019 Sesto Fiorentino, Firenze, Italy
- ⁵⁴University of Oregon, Eugene, OR 97403, USA
- ⁵⁵Laboratoire Kastler Brossel, ENS, CNRS, UPMC, Université Pierre et Marie Curie, F-75005 Paris, France
- ⁵⁶VU University Amsterdam, 1081 HV Amsterdam, The Netherlands
- ⁵⁷University of Maryland, College Park, MD 20742, USA
- ⁵⁸University of Massachusetts Amherst, Amherst, MA 01003, USA
- ⁵⁹Laboratoire des Matériaux Avancés (LMA), IN2P3/CNRS, Université de Lyon, F-69622 Villeurbanne, Lyon, France
- ⁶⁰Universitat de les Illes Balears—IEEC, E-07122 Palma de Mallorca, Spain
- ⁶¹Università di Napoli 'Federico II,' Complesso Universitario di Monte Sant'Angelo, I-80126 Napoli, Italy
- ⁶²Canadian Institute for Theoretical Astrophysics, University of Toronto, Toronto, Ontario, M5S 3H8, Canada
- ⁶³Tsinghua University, Beijing 100084, China
- ⁶⁴University of Michigan, Ann Arbor, MI 48109, USA
- ⁶⁵INFN, Sezione di Roma Tor Vergata, I-00133 Roma, Italy
- ⁶⁶National Tsing Hua University, Hsinchu Taiwan 300
- ⁶⁷Charles Sturt University, Wagga Wagga, NSW 2678, Australia
- ⁶⁸Caltech-CaRT, Pasadena, CA 91125, USA
- ⁶⁹Pusan National University, Busan 609-735, Korea
- ⁷⁰Australian National University, Canberra, ACT 0200, Australia
- ⁷¹Carleton College, Northfield, MN 55057, USA
- ⁷²Università di Roma Tor Vergata, I-00133 Roma, Italy
- ⁷³INFN, Gran Sasso Science Institute, I-67100 L'Aquila, Italy
- ⁷⁴Università di Roma 'La Sapienza', I-00185 Roma, Italy
- ⁷⁵University of Brussels, Brussels 1050, Belgium
- ⁷⁶Sonoma State University, Rohnert Park, CA 94928, USA
- ⁷⁷Texas Tech University, Lubbock, TX 79409, USA
- ⁷⁸University of Minnesota, Minneapolis, MN 55455, USA
- ⁷⁹The University of Sheffield, Sheffield S10 2TN, United Kingdom
- ⁸⁰Wigner RCP, RMKI, H-1121 Budapest, Konkoly Thege Miklós út 29-33, Hungary
- ⁸¹Montclair State University, Montclair, NJ 07043, USA
- ⁸²Argentinian Gravitational Wave Group, Cordoba Cordoba 5000, Argentina
- ⁸³Università di Trento, I-38123 Povo, Trento, Italy
- ⁸⁴INFN, Trento Institute for Fundamental Physics and Applications, I-38123 Povo, Trento, Italy
- ⁸⁵Northwestern University, Evanston, IL 60208, USA
- ⁸⁶University of Cambridge, Cambridge, CB2 1TN, United Kingdom
- ⁸⁷University of Szeged, Dóm tér 9, Szeged 6720, Hungary
- ⁸⁸Rutherford Appleton Laboratory, HSI, Chilton, Didcot, Oxon, OX11 0QX, United Kingdom
- ⁸⁹Embry-Riddle Aeronautical University, Prescott, AZ 86301, USA

- ⁹⁰The Pennsylvania State University, University Park, PA 16802, USA
⁹¹American University, Washington, DC 20016, USA
⁹²University of Adelaide, Adelaide, SA 5005, Australia
⁹³West Virginia University, Morgantown, WV 26506, USA
⁹⁴Raman Research Institute, Bangalore, Karnataka 560080, India
⁹⁵Korea Institute of Science and Technology Information, Daejeon 305-806, Korea
⁹⁶University of Białystok, 15-424 Białystok, Poland
⁹⁷SUPA, University of Strathclyde, Glasgow, G1 1XQ, United Kingdom
⁹⁸University of Southampton, Southampton, SO17 1BJ, United Kingdom
⁹⁹IISER-TVM, CET Campus, Trivandrum Kerala 695016, India
¹⁰⁰Institute of Applied Physics, Nizhny Novgorod, 603950, Russia
¹⁰¹Seoul National University, Seoul 151-742, Korea
¹⁰²Hanyang University, Seoul 133-791, Korea
¹⁰³NCBJ, 05-400 Świerk-Otwock, Poland
¹⁰⁴IM-PAN, 00-956 Warsaw, Poland
¹⁰⁵Institute for Plasma Research, Bhat, Gandhinagar 382428, India
¹⁰⁶The University of Melbourne, Parkville, VIC 3010, Australia
¹⁰⁷INFN, Sezione di Padova, I-35131 Padova, Italy
¹⁰⁸Monash University, Victoria 3800, Australia
¹⁰⁹ESPCI, CNRS, F-75005 Paris, France
¹¹⁰Università di Camerino, Dipartimento di Fisica, I-62032 Camerino, Italy
¹¹¹Southern University and A&M College, Baton Rouge, LA 70813, USA
¹¹²College of William and Mary, Williamsburg, VA 23187, USA
¹¹³Abilene Christian University, Abilene, TX 79699, USA
¹¹⁴Instituto de Física Teórica, University Estadual Paulista/ICTP South American Institute for Fundamental Research, São Paulo SP 01140-070, Brazil
¹¹⁵IISER-Kolkata, Mohanpur, West Bengal 741252, India
¹¹⁶Whitman College, 280 Boyer Ave, Walla Walla, WA 9936, USA
¹¹⁷National Institute for Mathematical Sciences, Daejeon 305-390, Korea
¹¹⁸Rochester Institute of Technology, Rochester, NY 14623, USA
¹¹⁹Hobart and William Smith Colleges, Geneva, NY 14456, USA
¹²⁰Tata Institute for Fundamental Research, Mumbai 400005, India
¹²¹SUPA, University of the West of Scotland, Paisley, PA1 2BE, United Kingdom
¹²²Institute of Astronomy, 65-265 Zielona Góra, Poland
¹²³Universität Hamburg, D-22761 Hamburg, Germany
¹²⁴Indian Institute of Technology, Gandhinagar Ahmedabad Gujarat 382424, India
¹²⁵Andrews University, Berrien Springs, MI 49104, USA
¹²⁶Trinity University, San Antonio, TX 78212, USA and
¹²⁷University of Washington, Seattle, WA 98195, USA

Draft version August 5, 2021

ABSTRACT

We describe directed searches for continuous gravitational waves in data from the sixth LIGO science data run. The targets were nine young supernova remnants not associated with pulsars; eight of the remnants are associated with non-pulsing suspected neutron stars. One target’s parameters are uncertain enough to warrant two searches, for a total of ten. Each search covered a broad band of frequencies and first and second frequency derivatives for a fixed sky direction. The searches coherently integrated data from the two LIGO interferometers over time spans from 5.3–25.3 days using the matched-filtering \mathcal{F} -statistic. We found no evidence of gravitational-wave signals. We set 95% confidence upper limits as strong (low) as 4×10^{-25} on intrinsic strain, 2×10^{-7} on fiducial ellipticity, and 3×10^{-6} on r -mode amplitude. These beat the indirect limits from energy conservation and are within the range of theoretical predictions for neutron-star ellipticities and r -mode amplitudes.

Keywords: gravitational waves — stars: neutron — supernova remnants

1. INTRODUCTION

Young neutron stars are attractive targets for searches for continuous gravitational waves (GWs) even if they are not detected as pulsars (Wette et al. 2008; Owen 2009; Abadie et al. 2010). Some are seen as non-pulsing central compact objects (CCOs) in supernova remnants (SNRs), and some young pulsar wind nebulae (PWNe) and SNRs indicate the location of a young neutron star with enough precision for a directed search—a search over frequency and spin-down parameters, but not over sky positions. Some young pulsars spin fast enough to emit GWs in the frequency band of ground-based interferometers such as the Laser Interferometer Gravitational-wave Observatory (LIGO) and Virgo, and therefore some young non-pulsars may also spin fast enough. Even without observed pulsations and spin-down parameters, it is pos-

sible to estimate an indirect upper limit on GW emission, analogous to the spin-down limit (Shklovskii 1969) for known pulsars, based on the age of and distance to the star plus energy conservation (Wette et al. 2008). Given the great uncertainties in predictions of GW emission from young neutron stars, we use this indirect limit rather than those predictions to pick targets for directed searches.

We describe such searches of data from the sixth LIGO science run (S6) for continuous GWs from Cas A and eight more supernova remnants with known or suspected young isolated neutron stars with no observed electromagnetic pulsations. These targets were chosen so that a computationally feasible coherent search similar to Abadie et al. (2010) could beat the indirect limits on GW emission. Therefore each search had a chance of

detecting something, and non-detections could constrain the star’s GW emission, provided that emission is at a frequency in the band searched. No search found evidence for a GW signal, and hence the main result is a set of upper limits similar to those presented in Abadie et al. (2010). These upper limits on GW emission translate into upper limits on the fiducial ellipticity and r -mode amplitude of each neutron star as a function of GW frequency the star could be emitting (see Subsection 3.2). The ellipticity and r -mode upper limits set by the searches described here were within the ranges of theoretical predictions (Johnson-McDaniel 2013; Bondarescu et al. 2009), another indicator that these searches reached interesting sensitivities (see Section 4).

For context, we compare to the other continuous GW searches, which correspond to three other astronomical populations that nonetheless share astrophysical emission mechanisms and other properties (Owen 2009). Directed searches occupy a middle ground between all-sky searches and targeted searches for known pulsars in the key tradeoff for continuous waves: Searches with greater sensitivity and less computational cost require more astronomical information, and have different indirect limits to beat to reach an interesting sensitivity.

The first search for continuous waves in LIGO data, from its first science run (S1), was for a single known pulsar (Abbott et al. 2004). Such a search, guided by a precise timing solution, is computationally cheap and achieves the best strain sensitivity for a given amount of data since all available data can be integrated coherently. Since then, searches of data up to S6 have targeted up to 195 pulsars (Abbott et al. 2005b, 2007c, 2008b; Abadie et al. 2011a; Abbott et al. 2010; Aasi et al. 2014c). The four most recent of these papers set direct upper limits on GW emission stricter than the spin-down limits derived from energy conservation, for a few of the pulsars searched, thereby marking the point at which LIGO and Virgo began revealing new information about these pulsars. The upper limits also corresponded to neutron-star ellipticities within the range of theoretical predictions for exotic equations of state (Owen 2005).

Other continuous GW searches have surveyed the whole sky for neutron stars not seen as pulsars, using great computational power to cover wide frequency bands and large ranges of spin-down parameters (Abbott et al. 2005a, 2007a, 2008a, 2009a,b,c; Abadie et al. 2012; Aasi et al. 2013b, 2014a,d) and recently possible binary parameters too (Aasi et al. 2014b). Several of the recent all-sky searches have set direct upper limits competitive with indirect upper limits based on simulations of the galactic neutron-star population (Knispel & Allen 2008).

Between these two extremes of computational cost and sensitivity are the directed searches, where the sky location (and thus the detector-frame Doppler modulation) is known but the frequency and other parameters are not. Directed searches can be divided further into searches for isolated neutron stars (the type of search described in this paper), and searches for neutron stars in binary systems, with particular emphasis on accreting neutron stars in close (low mass x-ray) binaries. For accreting neutron stars, a different indirect limit can be set based on angular momentum con-

servation (Papaloizou & Pringle 1978). Unlike the energy conservation-based indirect limits for other neutron star populations, there is an argument (partially based on observations) that accreting neutron stars emit close to their limit, which also corresponds to reasonable ellipticities and r -mode amplitudes (Bildsten 1998). So far the only accreting neutron star targeted has been the one in the low-mass X-ray binary Sco X-1 (Abbott et al. 2007a,b; Abadie et al. 2011b; Aasi et al. 2015c). Searches for this object must cover not only a range of GW frequencies since no pulsations are observed, but also a range of orbital parameters since there are substantial uncertainties in these. Direct upper limits from searches for Sco X-1 have not beaten the indirect limit derived from accretion torque balance (Papaloizou & Pringle 1978), but may with data from interferometers upgraded to the “advanced” sensitivity (Harry 2010; Aasi et al. 2015a; Sammut et al. 2014).

The type of directed search described here, for isolated neutron stars not seen as pulsars, was first performed on data from the fifth LIGO science run (S5) for the CCO in the SNR Cas A (Abadie et al. 2010). Since then similar searches, using different data analysis methods, have been performed for supernova 1987A and unseen stars near the galactic center (Abadie et al. 2011b; Aasi et al. 2013a). Directed searches for isolated neutron stars are intermediate in cost and sensitivity between targeted pulsar searches and all-sky searches because a known sky direction allows for searching a wide band of frequencies and frequency derivatives with much less computing power than the all-sky wide-band searches (Wette et al. 2008) and no search over binary parameters is needed. The indirect limits to beat are numerically similar to those for known pulsars—the strain limit for Cas A is almost identical to that for the Crab pulsar. One disadvantage this type of search has compared to pulsar searches is that the spin frequencies of the neutron stars are not known. Based on pulsar statistics, it is likely that most of these stars are not spinning fast enough to be emitting GWs in the detectable frequency band, making it all the more important to search multiple targets. Here we improve the methods of the S5 Cas A search (Abadie et al. 2010) and extend our search targets to nine young supernova remnants total.

The rest of this article is structured as follows: In Sec. 2 we present the methods, implementation, and results of the searches. The upper limits set in the absence of evidence for a signal are presented in Sec. 3, and the results are discussed in Sec. 4. In the Appendix we describe the performance of the analysis pipeline on hardware injected signals.

2. SEARCHES

2.1. Data selection

S6 ran from July 7 2009 21:00:00 UTC (GPS 931035615) to October 21 2010 00:00:00 UTC (GPS 971654415). It included two interferometers with 4-km arm lengths, H1 at LIGO Hanford Observatory (LHO) near Hanford, Washington and L1 at LIGO Livingston Observatory (LLO) near Livingston, Louisiana. It did not include the 2-km H2 interferometer that was present at LHO during earlier runs. Plots of the noise power spectral density (PSD) curves and descriptions of the

Table 1

Target objects and astronomical parameters used in each search

SNR (G name)	Other name	RA+dec (J2000)	D (kpc)	a (kyr)
1.9+0.3		174846.9–271016	8.5	0.1
18.9–1.1		182913.1–125113	2	4.4
93.3+6.9	DA 530	205214.0+551722	1.7	5
111.7–2.1	Cas A	232327.9+584842	3.3	0.3
189.1+3.0	IC 443	061705.3+222127	1.5	3
266.2–1.2	Vela Jr.	085201.4–461753	0.2	0.69
266.2–1.2	Vela Jr.	085201.4–461753	0.75	4.3
291.0–0.1	MSH 11–62	111148.6–603926	3.5	1.2
347.3–0.5		171328.3–394953	0.9	1.6
350.1–0.3		172054.5–372652	4.5	0.6

Values of distance D and age a are at the optimistic (nearby and young) end of ranges given in the literature, except for the second search for Vela Jr. See text for details and references.

improvements over S5 can be found, for example, in Aasi et al. (2015b). A description of the calibration and uncertainties can be found in Bartos et al. (2011). The phase calibration errors at the frequencies searched were up to 7° and 10° for H1 and L1 respectively, small enough not to affect the analysis. The corresponding amplitude calibration errors were 16% and 19% respectively. For reasons discussed in Aasi et al. (2014c) we estimate the maximum amplitude uncertainty of our joint H1-L1 results to be 20%.

Concurrently with the LIGO S6 run, the Virgo interferometer near Cascina, Italy had its data runs VSR2 and VSR3. Although Virgo noise performance was better than LIGO in a narrow band below roughly 40 Hz, it was worse than LIGO by a factor 2–3 in amplitude at the higher frequencies of the searches described here. Virgo’s declination response function for many-day observations averaged over inclinations and polarizations is within about 10 percent of that of LHO, and even extreme inclinations and polarizations are not too far from average [see Fig. 4 and Eq. (86) respectively of Jaranowski et al. (1998)]. Hence Virgo’s single-interferometer sensitivity is worse by a factor 2–3 in amplitude, and since the signal-to-noise is added in quadrature between interferometers, the addition of Virgo would enhance the sensitivity to a typical source by at most a few percent—much less than the LIGO calibration uncertainty. Since data analysis costs the same for all interferometers and computational resources are limited, the searches described here used only LIGO data.

Like many other continuous-wave searches, those reported here used GW data in the SFT format. The series of science-mode data, interrupted by planned (maintenance) and unplanned downtime (earthquakes etc.), minus short segments which were “category 1” vetoed (Aasi et al. 2015b), was broken into segments of $T_{\text{SFT}} = 1800$ s. There were a total of 19 268 of these segments for H1 and L1 during the S6 run. Each 30-minute segment was first high pass filtered in the time domain through a tenth order Butterworth filter with a knee frequency of 30 Hz to attenuate low frequency seismic noise. Then it was Tukey windowed with parameter 0.001 (i.e. only 0.1% of samples were modified) to mitigate edge artifacts. Finally each segment was Fourier transformed and frequencies from 40–2035 Hz were recorded in the corre-

sponding SFT.

Although a directed search is computationally more tractable than an all-sky search, computational costs nonetheless restricted us to searching a limited time span T_{span} of the S6 data. This span, and the frequency band $f_{\text{min}}-f_{\text{max}}$, were determined for each target by an algorithm designed to fix the computational cost per target as described in Subsection 2.4. The data selection criterion was the same as in Abadie et al. (2010), maximizing the figure of merit

$$\sum_{f,t} \frac{1}{S_h(f,t)} \quad (1)$$

where the sums run over the given T_{span} , f_{min} , and f_{max} for each target. Here f is the frequency of each bin (discretized at $1/T_{\text{SFT}}$), t is the time stamp of each SFT, and S_h is the strain noise PSD harmonically averaged over the H1 and L1 interferometers. Maximizing this figure of merit roughly corresponds to optimizing (minimizing) the detectable GW strain, harmonically averaged over the frequency band. Although the frequency band for each search varied target by target, the sum was dominated by the least noisy frequencies that are searched for all targets, and thus the optimization always picked time spans near the end of S6 when the noise at those frequencies was best (least) and the SFT duty factor (total SFT time divided by T_{span} divided by numbers of interferometers [two]) was highest. This figure of merit also neglects the small effect where LHO is better for high declination sources and LLO is better for low (Jaranowski et al. 1998). Since the optimal data stretches tended to have comparable amounts of H1 and L1 data, the declination effect was at most a few percent, less than the amplitude calibration uncertainties.

2.2. Analysis method

The analysis was based on matched filtering, the optimal method for detecting signals of known functional form. To obtain that form we assumed that the instantaneous frequency of the continuous (sinusoidal) GWs in the solar system barycenter was

$$f(t) \simeq f + \dot{f}(t - t_0) + \frac{1}{2}\ddot{f}(t - t_0)^2. \quad (2)$$

That is, we assumed that none of the target neutron stars glitched (had abrupt frequency jumps) or had significant timing noise (additional, perhaps stochastic, time dependence of the frequency) during the observation. We also neglected third and higher derivatives of the GW frequency, based on the time spans and ranges of \dot{f} and \ddot{f} covered. The precise expression for the interferometer strain response $h(t)$ to an incoming continuous GW also includes amplitude and phase modulation by the changing of the beam patterns as the interferometer rotates with the earth. It depends on the source’s sky location and orientation angles, as well as on the parameters of the interferometer, and takes the form of four sinusoids. We do not reproduce the lengthy expression here, but it can be found in Jaranowski et al. (1998).

The primary detection statistic was the multi-interferometer \mathcal{F} -statistic (Cutler & Schutz 2005). This is based on the single-interferometer \mathcal{F} -statistic (Jaranowski et al. 1998), which combines the results of

Table 2
Derived parameters used in each search

SNR (G name)	f_{\min} (Hz)	f_{\max} (Hz)	T_{span} (s)	T_{span} (days)	Start of span (UTC, 2010)	H1 SFTs	L1 SFTs	Duty factor
1.9+0.3	141	287	788 345	9.1	Aug 22 00:23:45	356	318	0.77
18.9–1.1	132	298	2 186 572	25.3	Aug 13 02:02:24	786	912	0.70
93.3+6.9	109	373	2 012 336	23.3	Aug 10 18:49:49	770	813	0.71
111.7–2.1	91	573	730 174	8.4	Aug 22 10:27:49	332	289	0.77
189.1+3.0	101	464	1 553 811	18.0	Aug 13 07:55:32	650	634	0.74
266.2–1.2	46	2034	456 122	5.3	Jul 30 06:17:12	218	186	0.80
266.2–1.2	82	846	1 220 616	14.1	Aug 17 02:58:47	525	503	0.76
291.0–0.1	124	315	1 487 328	17.2	Aug 14 00:53:35	629	615	0.75
347.3–0.5	82	923	903 738	10.5	Aug 20 22:00:05	397	370	0.76
350.1–0.3	132	301	1 270 309	14.7	Aug 16 13:10:34	538	519	0.75

The span reported is the final one, including the possible extension to the end of an Short Fourier Transform (SFT) in progress at the end of the originally requested span. The duty factor reported is total SFT time divided by T_{span} divided by the number of interferometers (two).

matched filters for the four sinusoids of the signal in a way that is computationally fast and nearly optimal (Prix & Krishnan 2009). In Gaussian noise $2\mathcal{F}$ is drawn from a χ^2 distribution with four degrees of freedom, and hence $\mathcal{F}/2$ is roughly a power signal-to-noise ratio.

We used the implementation of the \mathcal{F} -statistic in the LALSuite package, tag `S6SNRSearch`, publicly available at <https://www.lsc-group.phys.uwm.edu/daswg/projects/lalsuite.html>. In particular most of the computing power of the search was spent in the `ComputeFStatistic_v2_SSE` program, which unlike the version used in the preceding search of this type (Abadie et al. 2010) uses the Intel SSE2 floating-point extensions and only 8 terms rather than 16 in the Dirichlet kernel. Both of these changes sped up the analysis (see below).

The algorithm for setting up a “template bank,” or choosing discrete points in the parameter space of (f, \dot{f}, \ddot{f}) to search, was the same as in Abadie et al. (2010). The “mismatch” or maximum loss of $2\mathcal{F}$ due to discretization of the frequency and derivatives (Owen 1996; Brady et al. 1998) was 0.2, again the same as in Abadie et al. (2010). Choosing to keep the computational cost the same for all searches resulted in some variation of the total number of templates per search, $3\text{--}12 \times 10^{12}$ compared to the 7×10^{12} in Abadie et al. (2010).

2.3. Target objects

The goal of these searches was to target young non-pulsing neutron stars. Starting with the comprehensive catalog of SNRs (Green 2009, 2014), augmented by a search of the recent literature, we narrowed the list to remnants with confirmed associated non-pulsing “point” sources—CCOs (mostly soft thermal emission, no radio, sub-arcsecond size) or small PWNe (mostly hard nonthermal emission, sub-arcminute size) or candidates. These strongly indicate the presence of a neutron star, although they do not indicate if it is emitting in the LIGO frequency band. We make our searches in the hopes that some of the stars are emitting in this band. We also included SNR G1.9+0.3, although a point source is not visible (and may not exist since the supernova may have been Type Ia), because this remnant is the youngest known and is small enough to search with a single sky location.

The final selection of target objects and search parameters was based on beating the indirect upper limit on GW emission due to energy conservation. This upper limit is based on the optimistic assumption that all of the star’s (unobserved) spin-down is due to GW emission, and has been since the supernova. In terms of the “intrinsic strain amplitude” h_0 defined by Jaranowski et al. (1998), this indirect limit is (Wette et al. 2008)

$$h_0 < 1.26 \times 10^{-24} \left(\frac{3.30 \text{ kpc}}{D} \right) \left(\frac{300 \text{ yr}}{a} \right)^{1/2}, \quad (3)$$

where D is the distance to the source and a is its age. This assumes a moment of inertia 10^{45} g cm^2 and (spherical harmonic $m = 2$) mass quadrupole GW emission, the usual assumptions in the GW literature; and also assumes that the star has spun down at least 10–20% since birth, the usual assumption in the pulsar literature. For current quadrupole (r -mode) emission, the indirect limit on h_0 is slightly higher (Owen 2010); but we used the mass quadrupole value. The intrinsic strain h_0 is generally a factor 2–3 greater than the actual strain amplitude response of a detector; it is defined precisely in Jaranowski et al. (1998) and related to standard multipoles and properties of the source in Owen (2010). It can be converted to fiducial ellipticity and r -mode amplitude of a neutron star via Eqs. (7) and (8). In order to beat the limit (3) over as wide a frequency band as possible, we generally used the most optimistic (lowest) age and distance estimates from the literature, corresponding to the highest indirect limit, with exceptions noted below. The algorithm for that final selection is described in the next subsection.

The resulting target list and astronomical parameters are shown in Table 1. The individual SNRs and the provenance of the parameters used are:

G1.9+0.3—Currently the youngest known SNR in the galaxy (Reynolds et al. 2008). Nothing is visible inside the remnant, which although more than an arcminute across is small enough to be searched with one sky position for the integration times used here (Whitbeck 2006). Several arguments favor it being a Type Ia (Reynolds et al. 2008), which would leave no neutron star behind, but this is not definite and the remnant’s youth makes it an interesting target on the chance it is

not Type Ia. We used the position of the center of the remnant from the discovery paper (Reich et al. 1984). The age and distance are from the “rediscovery” paper (Reynolds et al. 2008).

G18.9-1.1—The position is that of the *Chandra* point source discovered by Tüllmann et al. (2010). There is also an x-ray and radio PWN candidate trailing back toward the center of the SNR (Tüllmann et al. 2010). Age and distance estimates are from Harrus et al. (2004).

G93.3+6.9—Also known as DA 530. The position and age are from Jiang et al. (2007). No true (sub-arcsecond) *Chandra* point source is seen, but since the x-ray and radio PWN candidate is barely detected in x-rays and the SNR overall is anomalously faint in x-rays, it is plausible that the pulsar powering the nebula is weak and remains to be detected in the brightest part of the PWN. The e-folding scale of X-ray intensity at the center of the PWN candidate is 6”, which qualifies as a point source for the GW search. The distance estimate is from Foster & Routledge (2003).

G111.7-2.1—Also known as Cas A. The point source is the prototypical CCO and was discovered with *Chandra*’s first light (Tananbaum 1999). The position is from that reference, the distance from Reed et al. (1995), the age from Fesen et al. (2006). In this search we used 300 years rather than 330 years as in Abadie et al. (2010), reflecting the idea of using optimistic ends of ranges given in the literature, which also corresponds to broader parameter space coverage. There is no evidence for a PWN, indicating that the neutron star may be slowly spinning or (better for GW emission) that it may have a weak surface magnetic field.

G189.1+3.0—Also known as IC 443. The position is that of the *Chandra* point source found by Olbert et al. (2001). It is a CCO-like object, though not at the center of the remnant, buried in a comet-shaped x-ray, radio, and possibly γ -ray PWN. This object is often studied, with a wide range of distance and age estimates in the literature. We used Petre et al. (1988) for an optimistic age estimate. We did not use the most optimistic distance quoted, but the assumed association with the I Gem cluster from Fesen & Kirshner (1980).

G266.2-1.2—Also known as Vela Jr. The position is that of the *Chandra* point source found by Pavlov et al. (2001). It is a CCO with no evidence of a PWN. The literature on this object also features a wide range of age and distance estimates, enough that we performed two searches (“wide” and “deep”). We used Iyudin et al. (1998) for the most optimistic age and distance, which were used in the wide search. The more pessimistic numbers, for the deep search, are from Katsuda et al. (2008). Even more extreme numbers have been quoted in the literature, but we restricted ourselves to those publications that contained some derivations of the numbers. [This was true at the time the computations were performed: As this manuscript was about to be submitted, a manuscript with derivations of more pessimistic numbers was made public (Allen et al. 2015).]

G291.0-0.1—Also known as MSH 11-62. The position and age are from the *Chandra* point source discovery paper (Slane et al. 2012). The distance is from Moffett et al. (2001). The age and distance are derived in slightly inconsistent ways, but rather than attempt to repeat the calculations we stuck to the numbers quoted

Table 3
Outliers warranting manual investigation

Search	Job min. and max. frequency (Hz)		Note
G18.9-1.1	192.470	192.477	Pulsar 8
G189.1+3.0	393.167	393.176	H1 & L1 clock noise
G189.1+3.0	399.264	399.272	L1 clock noise
G266.2-1.2 wide	441.004	441.212	H1 geophone
G266.2-1.2 wide	1397.720	1397.780	Pulsar 4
G266.2-1.2 wide	1408.100	1408.170	H1 electronics
G347.3-0.5	108.790	108.920	Pulsar 3
G347.3-0.5	192.448	192.522	Pulsar 8
G350.1-0.3	192.465	192.472	Pulsar 8
G350.1-0.3	192.472	192.479	Pulsar 8

Search jobs that produced non-vetoed candidates above the 95% confidence (5% false alarm probability) Gaussian threshold, along with the most likely causes. Notes of the form “Pulsar *N*” refer to hardware-injected signals (see the Appendix). The others are described in the text. Frequencies are shown in the solar system barycenter frame at the beginning of each observation span.

in the literature. The point source is embedded in a powerful PWN seen in x-rays and radio and possibly γ rays, although the poor Fermi-LAT spatial resolution makes the latter identification uncertain (Slane et al. 2012).

G347.3-0.5—Mignani et al. (2008) obtained the sub-arcsecond position from archival *Chandra* data, although the CCO had been identified in ASCA data earlier (Slane et al. 1999). There is no evidence of a PWN. We used the distance from Cassam-Chenai et al. (2004) and the age from the proposed identification with a possible SN 393 (Wang et al. 1997). Although this identification may be problematic given the inferred properties of such a supernova, other age estimates are comparable (Fesen et al. 2012).

G350.1-0.3—Position and distance estimates are from the discovery paper of the *XMM-Newton* point source by Gaensler et al. (2008). This is a CCO candidate with no evidence of a PWN. The age is from *Chandra* observations Lovchinsky et al. (2011).

2.4. Target selection and search parameters

The final selection of targets involved estimating GW search sensitivities and computing costs to determine which objects could feasibly be searched well enough to beat the energy conservation limits on GW emission—see Eq. (3). The sensitivity of each search was worked out in two iterations.

The first iteration made an optimistic sensitivity estimate using the noise PSD harmonically averaged over all S6 and both LIGO interferometers. Writing the 95% confidence upper limit (see Section 3) on intrinsic strain h_0 as

$$h_0^{95\%} = \Theta \sqrt{\frac{S_h}{T_{\text{data}}}}, \quad (4)$$

where T_{data} is the total data live time, the first iteration used a threshold factor Θ of 28 to ensure that it was too optimistic and thus did not rule out any targets that the second iteration would find feasible. [The second iteration results are not sensitive to the precise Θ chosen in the first iteration, as long as the first iteration value is slightly lower than the true values, which are in the 30s

as was seen in Abadie et al. (2010) and in the results of the second iteration.]

For a given frequency, we chose the range of first and second frequency derivatives in the same manner as Abadie et al. (2010). That is, we assumed a range of braking indices $n = f\ddot{f}/\dot{f}^2$ from 2–7, so that

$$-\frac{f}{(n_{\min} - 1)a} \leq \dot{f} \leq -\frac{f}{(n_{\max} - 1)a} \quad (5)$$

at each frequency. For each (f, \dot{f}) the second derivative satisfied

$$\frac{n_{\min}\dot{f}^2}{f} \leq \ddot{f} \leq \frac{n_{\max}\dot{f}^2}{f}. \quad (6)$$

The physical reasoning behind these choices is explained further in Abadie et al. (2010). The goal is to cover observed braking indices plus a variety of predicted GW emission mechanisms whose relative importance may have changed over time. Note that the range of \dot{f} does not extend up to zero. This might seem to be an issue as it would not include “anti-magnetars”, or young neutron stars which are observed to spin down very slowly and hence must have small surface magnetic fields (Gotthelf & Halpern 2008). However, these are stars we would not detect anyway—any star with GW emission close enough to the indirect limit to be detected would have a high spin-down due to that emission, even if it had a low surface magnetic field.

The computational cost is a function of the parameter space covered. That functional dependence was used to choose the parameters of these searches and will be used in planning future searches. The product of the ranges on f , \dot{f} , and \ddot{f} suggests that the size of the parameter space and the computational cost should scale as $f_{\max}^3 a^{-3} T_{\text{span}}^7$ (Wette et al. 2008). In the limit that only one value of \dot{f} is used, the range of that parameter should be eliminated from the product, the parameter space should be two dimensional rather than three, and the scaling should be $f_{\max}^2 a^{-1} T_{\text{span}}^4$. By setting up several searches with different parameters perturbed from those of the Cas A search, we observed that the computational cost scaled roughly as $f_{\max}^{2.2} a^{-1.1} T_{\text{span}}^4$. Comparing this to Wette et al. (2008) shows that the effective dimensions of the template banks were nearly 2 rather than 3, as confirmed by the fact that the number of different \dot{f} values in the template banks was typically more than one but small.

Assuming a 70% duty factor, and the empirical scaling for computational cost above, we determined the three unknowns (f_{\min} , f_{\max} , T_{span}) by setting the sensitivity (4) equal to the indirect limit on h_0 (3) at both ends of the search frequency band (f_{\min} and f_{\max}). The third condition to fix the three unknowns was to keep the computational cost per search at roughly the same nominal value as Abadie et al. (2010), although because of hardware and software improvements the total computational time was less (see below).

The second iteration involved running the analysis pipeline on small bands to get true template densities, the noise PSD of the optimal data stretch for each search, upper limits, and thus a better estimate of each Θ . For at least a 10 Hz band near each f_{\min} and f_{\max} , we ran the search (without looking at detection candidates) to

get upper limits. We then read off the value of Θ [from the observed upper limits and inverting Eq. (4)] at frequencies near f_{\min} and f_{\max} . These values were spot checked beforehand to verify that upper limits were comparable to indirect limits. This second iteration was good enough, considering calibration uncertainties and other errors. The lowest (best) values of Θ were comparable to the 31.25 predicted by averaging the calculation of Wette (2012) over declination, but in some bands Θ could be more than 40 because of narrow noisy and/or non-stationary bands. In general Θ rose slightly at higher frequencies because of the increasing density of templates (per Hz).

Table 2 lists the targets and other GW search parameters determined by the sensitivity algorithm. These parameters were confirmed by several consistency checks:

For each search we checked that \dot{f} was the highest frequency derivative needed for the resulting T_{span} using the parameter-space metric of Whitbeck (2006). Specifically, we computed the diagonal metric component for the third frequency derivative and verified that the $2\mathcal{F}$ lost by neglecting that derivative in the worst corner of parameter space searched was much less than the 20% template bank mismatch: In the worst case, the Vela Jr. wide search, it was just under 1%.

For each search we also checked the “pixel size” obtained from the metric on the sky position parameters to verify that more than one sky position was not needed. The position error ellipses for a 20% mismatch were roughly 0.8–2 arcminutes across the minor axis for T_{span} of two weeks, and that width scaled as the inverse of T_{span} . Most of the target positions are known to sub-arcsecond accuracy. The location of the object in SNR G93.3+6.9 is known to a few arcseconds. SNR G1.9+0.3 has no known object inside, but the remnant itself is barely an arcminute across; and given the age and distance any neutron star would have moved only a few arcseconds from the center of the remnant even at transverse kick velocities of order 1000 km/s. Since the integration time for that SNR was short, the error ellipse was several arcminutes across.

We also confirmed that the standard 1800-second SFTs do not cause problems. The \mathcal{F} -statistic code requires that signals not change more than a frequency bin over the duration of an SFT. The maximum \dot{f} feasible is then $1/(1800 \text{ s})^2 \approx 3 \times 10^{-7} \text{ Hz/s}$. The strongest \dot{f} from orbital motion in these searches is $2 \text{ kHz} \times 10^{-4} \times 2\pi/1 \text{ yr} \approx 4 \times 10^{-8} \text{ Hz/s}$, where the 10^{-4} is the Earth’s orbital velocity in units of c . The strongest intrinsic spin-down is $2 \text{ kHz}/690 \text{ yr} \approx 9 \times 10^{-8} \text{ Hz/s}$. (Both of these figures come from the Vela Jr. wide search.)

2.5. Implementation

All searches ran on the Atlas computing cluster at the Max Planck Institute for Gravitational Physics (Albert Einstein Institute) in Hanover, Germany. Most searches used 140 000–150 000 computational core-hours on Intel Xeon 3220 processors, except the Vela Jr. wide search which used about 110 000. The costing algorithm became less accurate for that search because the effective dimensionality of the parameter space was closer to 3 than to 2, as the range of \dot{f} searched was more than usual. This will need to be accounted for in future searches over wide

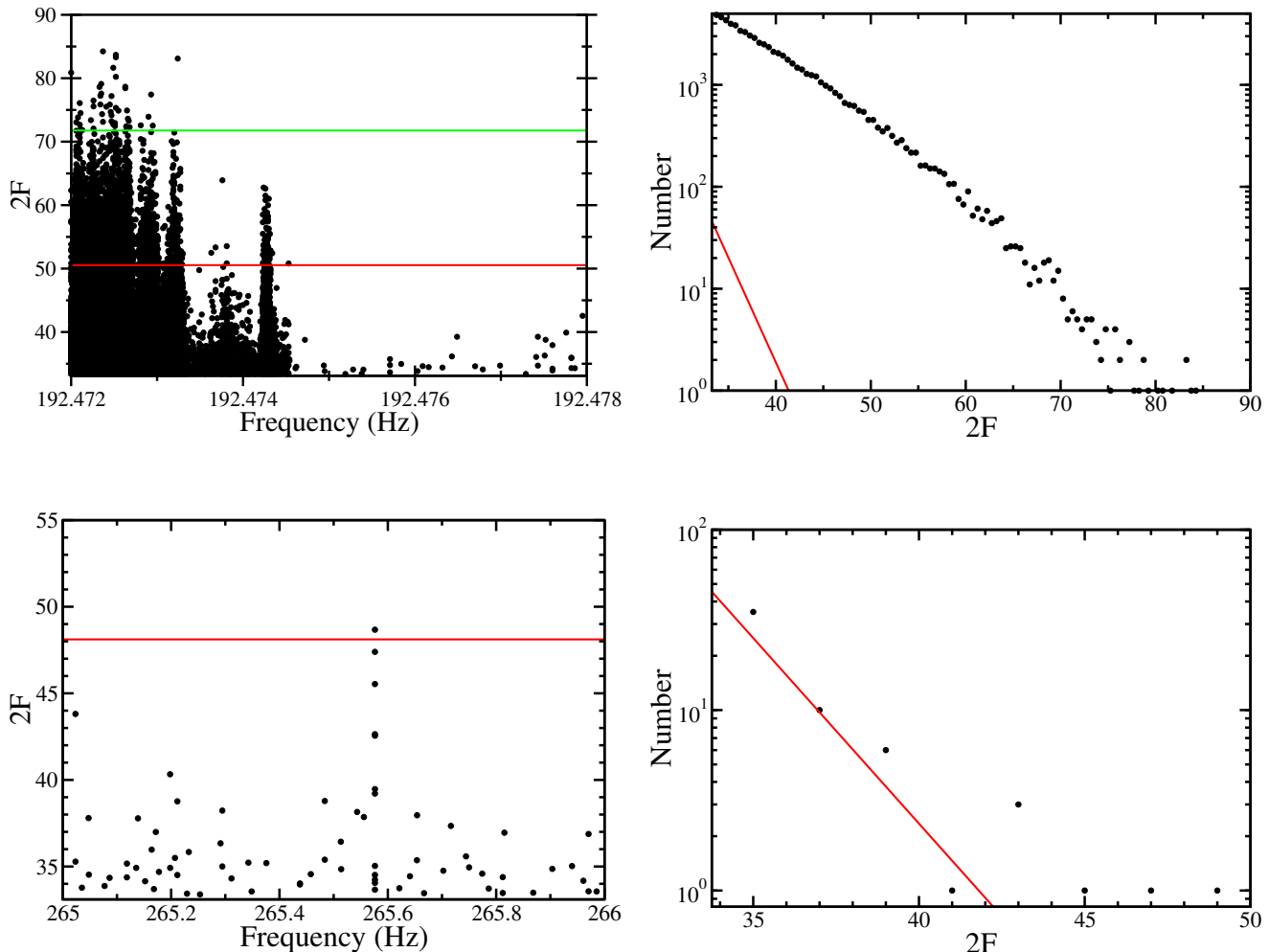


Figure 1. Inspection of the last outlier (top) and hardware-injected Pulsar 0 (bottom). Top left: $2\mathcal{F}$ vs. frequency for the search job. The higher line is the 95% confidence (5% false alarm) Gaussian threshold for the whole search; the lower line is the same for that search job. Top right: Histogram (tail) of $2\mathcal{F}$ for the search job. The line is for Gaussian noise, a χ^2 with four degrees of freedom. Bottom left: $2\mathcal{F}$ vs. frequency for the hardware injection search job; the line is the 95% confidence (5% false alarm) Gaussian threshold for that job. Bottom right: Histogram (tail) of $2\mathcal{F}$; the line is a χ^2 with four degrees of freedom.

bands and/or short spans. The number of matched filtering templates used in each search was about $3\text{--}12 \times 10^{12}$, comparable to the 7×10^{12} used in Abadie et al. (2010). The latter cost about 420 000 core-hours; the factor of 3 speed-up was due mainly to the SSE2 floating-point extensions used in the new code.

The way the search costs were split into cluster computing jobs affected the automated vetoes described in the next subsection. Each search was split into nominal 5-hour jobs, typically 28 000–30 000 jobs per search, except the Vela Jr. wide search which was about 22 000. In order to keep the search jobs at roughly the same computational cost, the frequency band covered by each job varied with frequency. The Vela Jr. wide search had jobs covering bands from 35 mHz to nearly 2 Hz at low frequencies, while the other searches had search job bands on the order of a few mHz to tens of mHz. Each search job recorded all candidates with $2\mathcal{F}$ above about 33.4, or 1 per million in stationary Gaussian white noise. In bands with “clean” noise, typical jobs with a few times 10^8 templates thus recorded a few hundred candidates. This choice of recording (which was different from the S5

search which recorded the loudest 0.01% of events) was needed to ease the manual investigation of outliers surviving the automated vetoes by making sure to record some noise at expected Gaussian levels. Such investigation was more important than in Abadie et al. (2010) because of the “dirtier” nature of the S6 noise and house-keeping issues associated with excessive disk space and input/output. The searches recorded a total of about 800 GB of candidates.

2.6. Vetoes

A high value of $2\mathcal{F}$ is not enough to claim a detection, since instrumental lines lead to non-Gaussian and/or non-stationary noise in many narrow frequency bands. Hence we vetoed many candidates before further investigating a few survivors.

First, we used an “Fscan veto” similar to the one used in Abadie et al. (2010). An Fscan is a normalized spectrogram formed from the SFTs. First it normalizes SFTs by scaling the power to the running median over 50 frequency bins, correcting for the bias between the finite-point running median and the mean. (While more complicated than simply normalizing to the mean, this pro-

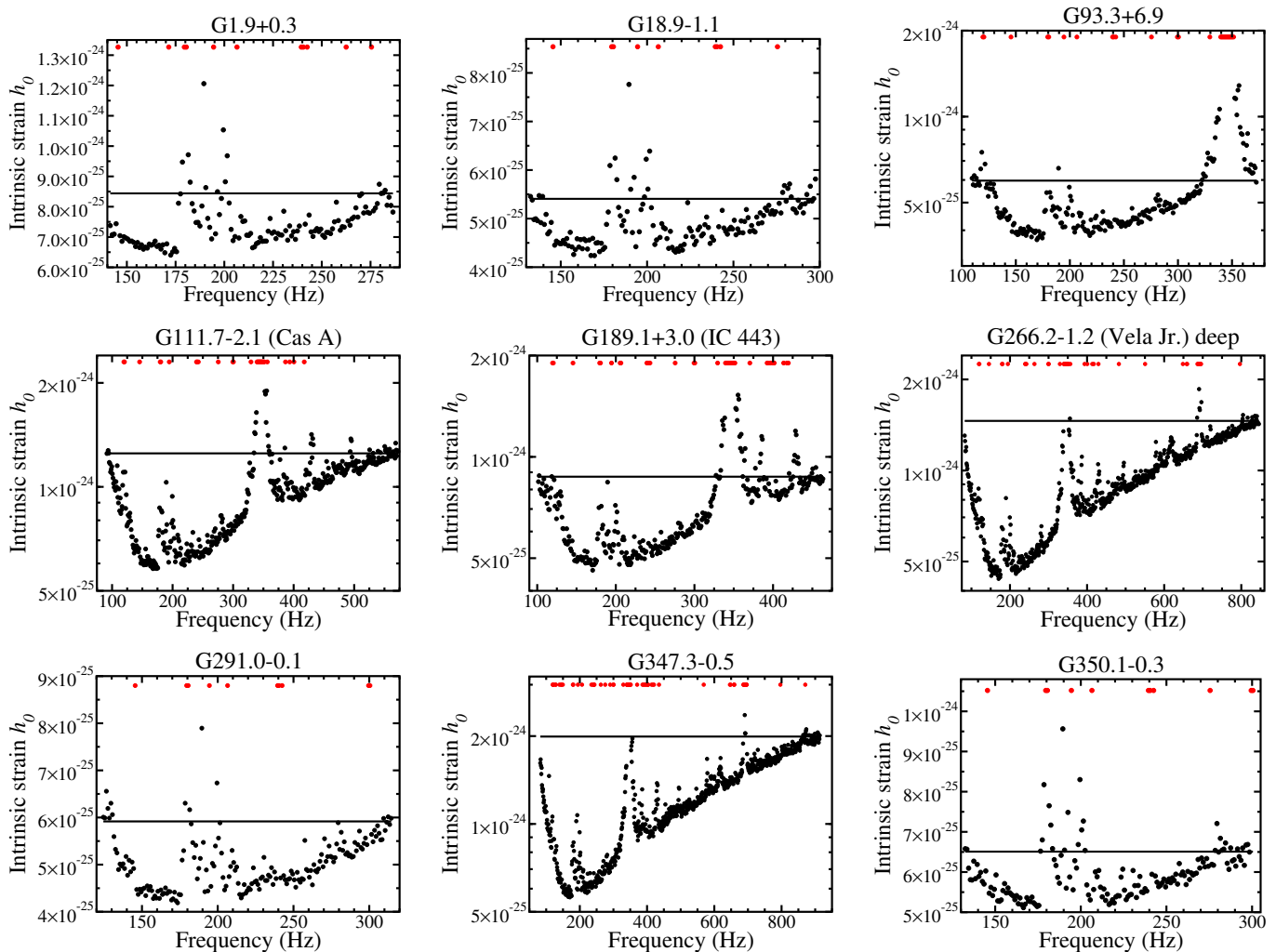


Figure 2. Direct observational upper limits (95% confidence, 5% false dismissal) on intrinsic strain h_0 are plotted as a function of frequency for all searches except the Vela Jr. wide search. They are shown as dots (black in the on-line version), each one representing an upper limit over a 1 Hz frequency band. Bands where no upper limit is set (see text) are given an artificial value so as to form a visibly distinguishable line of dots (in red in the on-line version) near the top of each plot. These bad bands consist of 5–10% of the total for each search. The solid horizontal lines are indirect limits on h_0 based on the ages of and distances to the remnants.

cedure is more robust to fluctuations in the time or frequency domain.) Then the Fscan time-averages the normalized power in each SFT frequency bin. In stationary Gaussian white noise the Fscan power for N_{SFT} SFTs is drawn from a χ^2 distribution with $2N_{\text{SFT}}$ degrees of freedom scaled to unit mean (thus having a variance N_{SFT}). Therefore deviations from a χ^2 indicate nonstationarity, spectral lines, or both.

In Abadie et al. (2010), the Fscan veto was triggered at a threshold of 1.5 times the expected power, which was about 11 standard deviations for H1 and 10.5 for L1. When triggered, it vetoed all signals overlapping a region 16 frequency bins on either side of the central frequency (the number of terms kept in the Dirichlet kernel) since those could be contaminated as well. Since the SSE2 code used here kept only 8 terms, we changed the window to 8 frequency bins.

In the present searches we also changed the threshold of the Fscan veto because we found that the S5 threshold was too lenient: S6 data had many more instrumental noise artifacts. Since the highest number of SFT frequency bins (in the Vela Jr. wide search) was

about 4×10^6 , an Fscan power threshold of six standard deviations above the mean and five below would be unlikely to veto any Gaussian noise. We increased the S6 threshold further to ± 7 standard deviations to allow for a roughly 3% bias (at most one standard deviation for these searches) observed in the Fscan power due to the effect of estimating the PSD with a running median over a finite number of bins (Prix 2009).

The second veto was based on the \mathcal{F} -statistic consistency veto introduced in Aasi et al. (2013b), which uses the fact that an astrophysical signal should have a higher joint value of $2\mathcal{F}$ (combining data from the two interferometers) than in either interferometer alone. Recorded candidates that violate this inequality were vetoed. This is a simpler and more lenient version of the more recent line veto (Keitel et al. 2014). In clean noise bands we found that it vetoed less than 1% of the candidates recorded.

We extended the consistency veto to limited frequency bands as follows: For each search job’s frequency band (minus any Fscan vetoed bands), if the number of candidates vetoed for consistency was greater than the number

of templates not vetoed, the entire search job was vetoed as being contaminated by a broad feature in one interferometer. Since we kept candidates at the 1 per million level for Gaussian noise, search jobs in clean noise bands recorded hundreds of templates, and hence this veto was only triggered if the number of consistency-vetoed candidates was about two orders of magnitude greater than usual.

The combination of these vetoes, although each was fairly lenient, greatly reduced the number of candidates surviving for human inspection. The vetoes also proved to be safe, in the sense that they were not triggered by the hardware-injected signals, with the exception of a few injections that were so loud that they distorted the data PSD and made it nonstationary (i.e. triggered the Fscan veto). It was easy to check that no astrophysical signals were vetoed this way by verifying that the small number of bands vetoed in both interferometers were due to the loud hardware-injected signals described in the Appendix or to known instrumental artifacts. The total frequency band vetoed was just over 1% of the frequency band searched, for all searches. We also checked with a full pipeline run of several hundred software injections and confirmed that, for $2\mathcal{F}$ less than about 230, about 1% went undetected due to vetoes.

2.7. Detection criteria and results

For each search, we computed the $2\mathcal{F}$ value corresponding to a 5% false alarm probability assuming Gaussian noise, and gave a further look to search jobs with nonvetoed candidates passing this threshold. Because of potential correlations between templates, we checked for an effective number of independent templates N_{eff} . The distribution of loudest nonvetoed event per search job for each target was nearly Gaussian. Therefore we determined N_{eff} by minimizing the Kolmogorov-Smirnov distance between the observed and expected cumulative distributions. For all searches this produced N_{eff} roughly 90% of the true number of templates and resulted in a further-look threshold of $2\mathcal{F} \approx 71-73$.

The search jobs that produced outliers surviving the automatic vetoes and thus warranting manual investigation are listed in Table 3. For all investigations it sufficed to make two plots of the results of the search job, demonstrated in Fig. 1 for the last outlier in Table 3 (top panels) and the first (and barely detected in 10 days' integration) hardware injection, ‘‘Pulsar 0’’ (bottom panels, see the Appendix for more on the hardware injections).

Examples of the first plot, of $2\mathcal{F}$ vs. frequency, are shown in the left-hand panels of Fig. 1. Injected signals showed up as near- δ -functions in this plot, as in the bottom left panel of Fig. 1, while noise outliers had broader structures as in the top left panel. In most cases the outliers are clearly leaking past the edges of a vetoed band. Most of the outliers were near those hardware-injected signals that were loud enough to trigger the Fscan veto.

The second plot used in each investigation was a histogram of the probability density function of the recorded candidates, exemplified in the right-hand panels of Fig. 1. All jobs with outliers surviving the veto process clearly showed the tail of a χ^2 distribution with the wrong normalization, as in the top right panel, indicating that the estimator of the noise PSD was off because of a narrow spectral feature or nonstationarity. Injected signals in

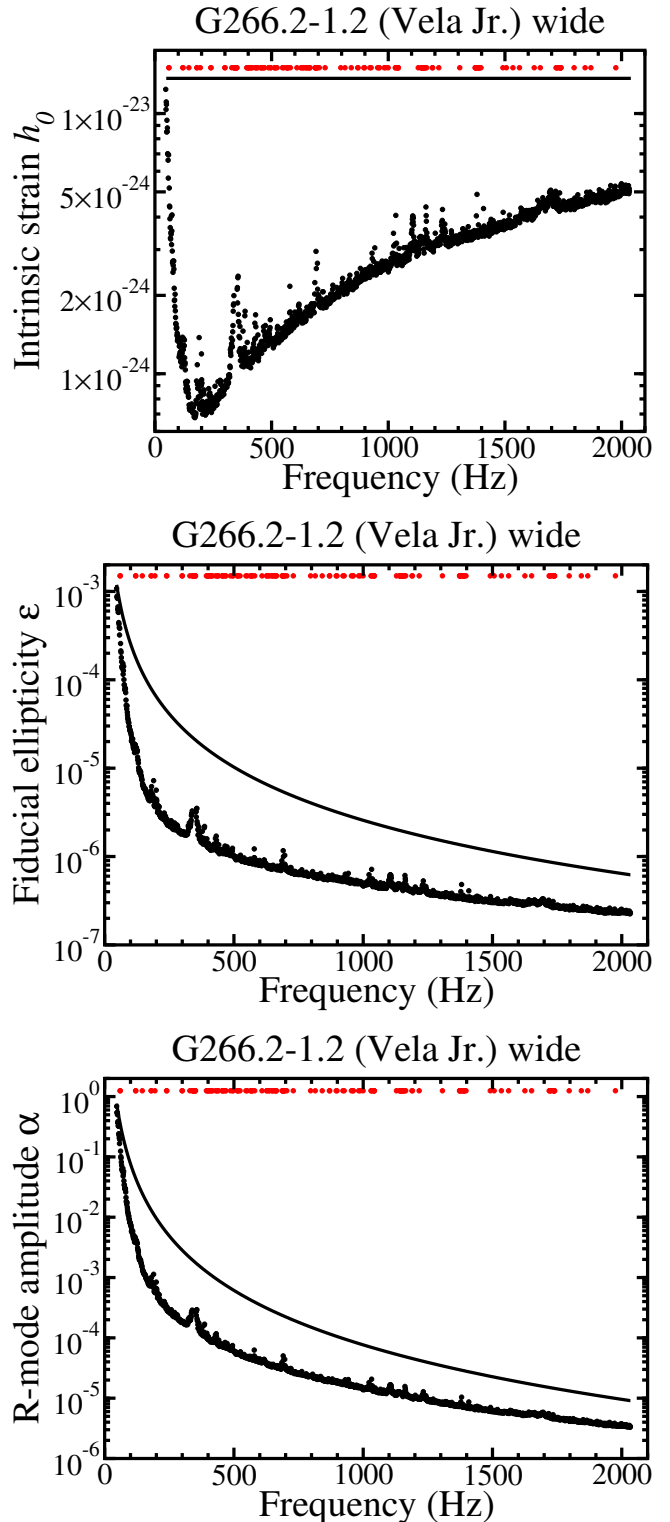


Figure 3. The top plot is the analog of Fig. 2 for the Vela Jr. wide search. The middle and bottom plots are the corresponding upper limits on fiducial ellipticity and r -mode amplitude.

clean data showed a correctly normalized χ^2 tail with a relatively small number of outliers extending to high $2\mathcal{F}$ values, which was visibly distinguishable from the candidates caused by noisy data, as can be seen in the bottom right panel.

We also tracked down the instrumental sources of the

outliers in Table 3. (This was done after the outliers had already been dismissed by the inspections above, and was directed toward improving future searches rather than adding confidence to the results of this one.) In all cases the search jobs producing outliers were adjacent in frequency to Fscan vetoed bands or consistency-vetoed search jobs, and the outliers were apparently produced by strong lines (including some very strong hardware injections) leaking past the vetoes (which were fairly lenient). Six of the outliers were associated with strong hardware injections, which appeared as broad spectral features rather than δ -functions due to residual Doppler modulation (since their sky positions did not match the positions being searched). Of the other outliers, the first two were associated with digital clock noise lines in both interferometers which drifted around bands of a few Hz. In the former outlier, the lines happened to coincide at the time of the observation; the latter outlier was just contributed by L1. In addition, there was an outlier associated with a 441 Hz calibration signal in a geophone prefilter in H1. The last non-injection outlier was part of a very stable and wide-ranging structure with dozens of sidebands seen in H1, identified also as digital electronic noise.

3. UPPER LIMITS

3.1. Methods

The method for setting upper limits was essentially the same as in Abadie et al. (2010). We divided each search into 1 Hz bands. For each of these upper limit bands, we recorded the loudest $2\mathcal{F}$ which passed the automated vetoes. We then estimated the intrinsic strain h_0 at which 95% of signals would be found, if drawn from a population with random parameters other than h_0 , with a louder value than the loudest $2\mathcal{F}$ actually recorded for that upper limit band. That is, we set a 5% false dismissal rate over a population of neutron stars randomly oriented and uniformly distributed over the 1 Hz band, with the loudest observed $2\mathcal{F}$ in that band setting the false alarm rate.

This 95% confidence limit was first estimated for each upper limit band with a combination of analytical and computationally cheap Monte Carlo methods. Then, in the more computationally intensive step (in some cases 20–30% of the cost of the original search), we software-injected 6 000 signals into the band at that h_0 to test that the confidence level was truly 95%. The frequencies of these software injections were randomly chosen within the band, and the polarization and inclination angles were chosen randomly. The upper limit injection runs have some safety margin built in, and in fact the confidence level was typically 96–97%. For a few upper limit bands—less than 1% of the total for each search—this test showed that the confidence level was actually lower than 95%. These typically corresponded to bands known to contain significant numbers of instrumental lines, and rather than iterate the computationally expensive procedure we chose not to present upper limits for these bands.

3.2. Results

The resulting upper limits on h_0 , in 1 Hz bands, are plotted in Figs. 2 and 3. They closely follow the shape

of the joint noise PSD, although with an overall scale factor and slight shape distortions. The best (lowest) upper limits on h_0 generally occur for each search around 170 Hz, where the noise PSD is lowest. Several searches achieved upper limits on h_0 of about 4×10^{-25} in that band, as can be seen in Table 4 (which also includes the indirect limits from energy conservation). Table 5 lists data for our observational upper limits on h_0 for all searches, i.e. the black points in Fig. 2 and the top panel of Fig. 3, in machine-readable form.

In all these plots, the main set of points does not include bands where more than 5% of the 1 Hz upper limit band is vetoed or where the injection-checked false dismissal rate was more than 5%. Most of these frequencies correspond to known instrumental disturbances, such as calibration lines or clock noise. We also removed 2 Hz bands centered on the electrical mains frequency of 60 Hz and its harmonics up to 300 Hz, as well as the band 339–352 Hz which is full of the extremely strong “violin modes” of the test mass suspension system. While a few upper limit bands containing these lines did pass the false dismissal and vetoed-band tests, the upper limits were much higher (weaker) on account of the increased noise; and upper limits on bands where the noise PSD varies greatly within the band are not so informative. Hence all these bad bands are removed from the main set of points, but are plotted near the top of each plot (in red on-line, at a constant h_0 in each plot) so as to give an idea of their numbers (5–10% of the total for each search) and locations (clustered around suspension violin modes, etc).

The strain upper limits can be converted to upper limits on the fiducial ellipticity $\epsilon = |I_{xx} - I_{yy}|/I_{zz}$ of each neutron star using (e.g. Wette et al. 2008)

$$\epsilon = 9.5 \times 10^{-5} \left(\frac{h_0}{10^{-24}} \right) \left(\frac{D}{1 \text{ kpc}} \right) \left(\frac{100 \text{ Hz}}{f} \right)^2, \quad (7)$$

assuming a fiducial value of $I_{zz} = 10^{45} \text{ g cm}^2$. We used this equation to convert both the energy-conservation limit and the direct 95% confidence limits obtained here. The results are plotted in the middle panel of Fig. 3 for the Vela Jr. wide search. This and the similar plots for the other searches are all tilted, curved versions of the plot for h_0 , and therefore we display only this one as an example. For all of the searches we summarize the ranges of ellipticity upper limits in Table 4.

Note that this fiducial ellipticity is really a dimensionless version of the (spherical harmonic $m = 2$ part of the) mass quadrupole moment, not the true shape of the star. Conversion factors to these other quantities can be found in Owen (2010) and Johnson-McDaniel (2013), respectively. The quantity truly inferred from the measurement of h_0 (and the measured frequency and assumed distance) is a component of the mass quadrupole. The conversion factor to ellipticity can have uncertainties of a factor 5 or more (Johnson-McDaniel 2013) depending on the neutron star mass, which has an observed range of about a factor 2, and the equation of state, which is significantly uncertain.

Strain upper limits can also be converted to limits on

Table 4
Upper limit summary

Search	Indirect h_0	Direct h_0	Direct ϵ		Direct α	
		lowest (best)	at f_{\min}	at f_{\max}	at f_{\min}	at f_{\max}
G1.9+0.3	8.4×10^{-25}	6.4×10^{-25}	2.9×10^{-4}	7.6×10^{-5}	6.2×10^{-2}	7.9×10^{-3}
G18.9-1.1	5.4×10^{-25}	4.2×10^{-25}	5.9×10^{-5}	1.2×10^{-5}	1.3×10^{-2}	1.2×10^{-3}
G93.3+6.9	6.0×10^{-25}	3.7×10^{-25}	8.1×10^{-5}	6.8×10^{-6}	2.2×10^{-2}	5.4×10^{-4}
G111.7-2.1	1.3×10^{-24}	5.8×10^{-25}	4.6×10^{-4}	1.2×10^{-5}	1.5×10^{-1}	6.2×10^{-4}
G189.1+3.0	8.7×10^{-25}	4.6×10^{-25}	1.2×10^{-4}	5.7×10^{-6}	3.4×10^{-2}	3.6×10^{-4}
G266.2-1.2 wide	1.4×10^{-23}	6.8×10^{-25}	1.1×10^{-3}	2.3×10^{-7}	6.9×10^{-1}	3.3×10^{-6}
G266.2-1.2 deep	1.5×10^{-24}	4.4×10^{-25}	1.4×10^{-4}	1.4×10^{-6}	4.9×10^{-2}	4.9×10^{-5}
G291.0-0.1	5.9×10^{-25}	4.2×10^{-25}	1.3×10^{-4}	2.0×10^{-5}	3.1×10^{-2}	1.9×10^{-3}
G347.3-0.5	2.0×10^{-24}	5.6×10^{-25}	2.0×10^{-4}	2.0×10^{-6}	7.3×10^{-2}	6.6×10^{-5}
G350.1-0.3	6.5×10^{-25}	5.1×10^{-25}	1.6×10^{-4}	3.1×10^{-5}	3.6×10^{-2}	3.1×10^{-3}

Here we summarize the range of upper limits set in these searches. The line for the G266.2-1.2 wide search summarizes the plots in Fig. 3 and the “Direct h_0 ” column summarizes the plots in Fig. 2. The remaining elements summarize similar results for the remaining searches which were not plotted. The best (lowest) upper limits on h_0 were set near 170 Hz for all searches, and the corresponding limits on α and ϵ were near the f_{\max} of each search.

Table 5
Upper limit data

Search	Frequency (Hz)	h_0 upper limit
G1.9+0.3	141.5	7.38×10^{-25}
G1.9+0.3	142.5	7.08×10^{-25}
G1.9+0.3	143.5	7.09×10^{-25}
G1.9+0.3	144.5	7.44×10^{-25}
...

This table lists data for our observational upper limits on h_0 for all searches, i.e. the black points in Fig. 2 and the top panel of Fig. 3. Frequencies are central frequencies for the upper limit bands. Only a portion of this table is shown here to demonstrate its form and content. A machine-readable version of the full table is available.

the r -mode amplitude α (Lindblom et al. 1998) via

$$\alpha = 0.028 \left(\frac{h_0}{10^{-24}} \right) \left(\frac{100 \text{ Hz}}{f} \right)^3 \left(\frac{D}{1 \text{ kpc}} \right), \quad (8)$$

for a typical neutron star, with about a factor 2–3 uncertainty depending on the mass and equation of state—see Eq. (24) of Owen (2010) and the discussion preceding it for details. We used this equation to convert both the energy-conservation limit and the direct 95% confidence obtained here. The results are plotted in the bottom panel of Fig. 3 for the Vela Jr. wide search. Like the plots of upper limits on fiducial ellipticity, the α upper limit plots are tilted, curved versions of the h_0 upper limit plots. Thus we do not display them for the other searches, although we do summarize all of the ranges in Table 4. Similarly to the case of fiducial ellipticity, the quantity most directly inferred from h_0 here is the ($m = 2$ part of the) current quadrupole. While α is a convenient dimensionless measure, the conversion factor—like that for ϵ —is uncertain by a factor of a few.

4. DISCUSSION

Our searches improved sensitivity and parameter space coverage over previous searches, beat indirect limits on GW emission from electromagnetic observations, and entered the range of theoretical predictions for neutron stars.

The best direct (observational) upper limits on h_0 and the indirect (theoretical) upper limits on h_0 from energy

conservation are shown in Table 4. The S5 search for Cas A (Abadie et al. 2010) obtained a best upper limit on h_0 of 7×10^{-25} . Our best S6 limit on Cas A was 6×10^{-25} , less of an improvement than the improvement in noise would indicate because we reduced the integration time. This in turn was because we searched a broader parameter space, including more than doubling the frequency band. Several of the S6 searches described here obtained upper limits on h_0 as strong (low) as 4×10^{-25} , nearly a factor of two better than Abadie et al. (2010) in spite of aiming in general for broad parameter space coverage. Several searches beat their corresponding indirect limits on h_0 by a factor of two, and the Vela Jr. wide search beat its indirect limit by about a factor of 20.

It is also interesting to compare our upper limits on neutron star fiducial ellipticities and r -mode amplitudes to the maximum values predicted theoretically. Although these predictions have many uncertainties, observational limits that beat them are more interesting than those that do not (even if the latter have beaten energy conservation limits). However we must be careful about interpreting GW emission limits as constraints on the physics of the targets—first of all, any target neutron star may just be spinning too slowly to emit in the frequency band searched. The spin frequency is half the GW frequency for mass quadrupole emission, or roughly three quarters for current quadrupoles (r -modes)—see Idrisy et al. (2015) for a more precise range of numbers for the latter. Each emission mechanism has a different range of predicted maximum quadrupoles. Depending on what is known about mechanisms for driving the quadrupoles toward maximum, we may set some constraints on individual neutron stars, although we cannot constrain universal properties such as the equation of state.

For mass quadrupoles supported by elastic forces, the analog of terrestrial mountains, we can say this: Many of our upper limits, summarized in Table 4, get well into the range for stars composed of normal nuclear matter rather than exotic alternatives, which has not been the case for previous GW searches. The most up-to-date numbers for elastically supported maximum quadrupoles are in Johnson-McDaniel & Owen (2013): They correspond to maximum fiducial ellipticities of order 10^{-5} for nor-

mal neutron stars, 10^{-3} for quark-baryon hybrid stars, and 10^{-1} for quark stars. For instance the Vela Jr. wide search beat a fiducial ellipticity of 10^{-5} over almost all of its frequency band. Since little is known about what processes could drive an elastic quadrupole toward its maximum in a young neutron star, we cannot use this information to constrain the composition or other properties of the neutron star or the properties of the processes.

Maximum values for magnetically supported mass quadrupoles depend on details of the field configuration such as the relative strengths of the poloidal and toroidal components as well as the hydrostatic structure of the star. Although the literature on the problem grows rapidly, the highest ellipticities predicted remain, as in Abadie et al. (2010), on the order of $10^{-4}(B/10^{15} \text{ G})^2$ —see Ciolfi & Rezzolla (2013) for a recent example and summary. Magnetic fields must deform the star, and hence there is a minimum deformation for a given internal field (found by varying the configuration) that does not greatly differ from the maximum (Mastrano et al. 2011). Thus our upper limits on h_0 correspond to upper limits on an average internal magnetic field if the object is emitting GW at the right frequency—for example, about 10^{14} G for the Vela Jr. wide search over much of its frequency band. While these internal field limits are high (magnetar strength), they do not require the objects to be magnetars since the external dipole fields could be much lower (Mastrano et al. 2011).

It is also interesting to compare to the largest r -mode amplitudes predicted by theory. This is also a complicated subject, depending on the history as well as the composition of the star. As at the time of Abadie et al. (2010), the most detailed calculation of nonlinear hydrodynamical saturation of the r -mode remains that of Bondarescu et al. (2009), and the answer is an amplitude of order 10^{-3} in terms of the quantity α used here. Thus, as seen in Fig. 3, the Vela Jr. wide search reached interesting values over most of its frequency band. And as seen in Table 3, most of the searches reached interesting values at least at the high end of their frequency bands. Since the GW-driven instability of the r -modes drives them towards saturation (Andersson 1998), probably even in realistic conditions for young neutron stars (Lindblom et al. 1998), these upper limits also have more constraining power than for elastic deformations: If an object is emitting in the frequency band searched but not detected, we can say that either the saturation amplitude is smaller or the damping mechanisms more effective than commonly thought; though due to the complicated physics of r -mode evolution scenarios it is difficult to be more precise.

In the near future, the Advanced LIGO and Virgo interferometers will come on-line and take data with strain

noise amplitude reduced from S6 values by a significant factor, which by the end of the decade will reach an order of magnitude. Re-running the analysis pipeline used here on such data would result in better sensitivity to h_0 , ϵ , and α by the same factor. Improved analysis methods are likely to improve the sensitivity even more, making it interesting (i.e. possible to detect a signal or at least to set upper limits that beat indirect limits) for many more supernova remnants and other targets.

The authors gratefully acknowledge the support of the United States National Science Foundation (NSF) for the construction and operation of the LIGO Laboratory, the Science and Technology Facilities Council (STFC) of the United Kingdom, the Max-Planck-Society (MPS), and the State of Niedersachsen/Germany for support of the construction and operation of the GEO600 detector, the Italian Istituto Nazionale di Fisica Nucleare (INFN) and the French Centre National de la Recherche Scientifique (CNRS) for the construction and operation of the Virgo detector. The authors also gratefully acknowledge research support from these agencies as well as by the Australian Research Council, the International Science Linkages program of the Commonwealth of Australia, the Council of Scientific and Industrial Research of India, Department of Science and Technology, India, Science & Engineering Research Board (SERB), India, Ministry of Human Resource Development, India, the Spanish Ministerio de Economía y Competitividad, the Conselleria d’Economia i Competitivitat and Conselleria d’Educació, Cultura i Universitats of the Govern de les Illes Balears, the Foundation for Fundamental Research on Matter supported by the Netherlands Organisation for Scientific Research, the Polish Ministry of Science and Higher Education, the FOCUS Programme of Foundation for Polish Science, the European Union, the Royal Society, the Scottish Funding Council, the Scottish Universities Physics Alliance, the National Aeronautics and Space Administration, the Hungarian Scientific Research Fund (OTKA), the Lyon Institute of Origins (LIO), the National Research Foundation of Korea, Industry Canada and the Province of Ontario through the Ministry of Economic Development and Innovation, the National Science and Engineering Research Council Canada, the Brazilian Ministry of Science, Technology, and Innovation, the Carnegie Trust, the Leverhulme Trust, the David and Lucile Packard Foundation, the Research Corporation, and the Alfred P. Sloan Foundation. The authors gratefully acknowledge the support of the NSF, STFC, MPS, INFN, CNRS and the State of Niedersachsen/Germany for provision of computational resources. This research has made use of the SIMBAD database, operated at CDS, Strasbourg, France. This paper has been designated LIGO document number LIGO-P1400182-v6.

APPENDIX

S6 featured a suite of hardware-injected continuous-wave signals, similar to previous science runs. Their nominal parameters (i.e. not allowing for calibration errors), in the notation of Jaranowski et al. (1998), are listed in Table 6. They are used by most searches, including those described here, for basic sanity checks of the analysis pipeline. For each of the first ten, called Pulsars 0–9, we searched a 1 Hz wide band around the injected frequency for a T_{span} of 10 days, and for Pulsar 0 we also did a 20 day search (see below). We did not search for Pulsars 10–12 since they were out of the frequency band of the SFTs we used. For each pulsar we ran the analysis pipeline using $f/|3\dot{f}|$ as the age so that the search would cover the injected spin-down parameter in roughly the middle of the range.

Table 6
Nominal hardware injection parameters

Pulsar No.	RA+dec (J2000)	Base frequency (Hz)	$-f$ (Hz/s)	h_0	ι (rad)	ψ (rad)	ϕ_0 (rad)
0	044612.5–561303	265.576360874	4.15×10^{-12}	2.47×10^{-25}	0.652	0.770	2.66
1	022934.5–292709	849.029489519	3.00×10^{-10}	1.06×10^{-24}	1.088	0.356	1.28
2	142101.5+032638	575.163548428	1.37×10^{-13}	4.02×10^{-24}	2.761	–0.222	4.03
3	115329.4–332612	108.857159397	1.46×10^{-17}	1.63×10^{-23}	1.652	0.444	5.53
4	183957.0–122800	1398.60769871	2.54×10^{-8}	4.56×10^{-23}	1.290	–0.648	4.83
5	201030.4–835021	52.8083243593	4.03×10^{-18}	4.85×10^{-24}	1.089	–0.364	2.23
6	235500.2–652521	147.511962499	6.73×10^{-9}	6.92×10^{-25}	1.725	0.471	0.97
7	145342.1–202702	1220.77870273	1.12×10^{-9}	2.20×10^{-24}	0.712	0.512	5.25
8	232533.5–332507	192.756892543	8.65×10^{-9}	1.59×10^{-23}	1.497	0.170	5.89
9	131532.5+754123	763.847316497	1.45×10^{-17}	8.13×10^{-25}	2.239	–0.009	1.01
10	144613.4+425238	26.3588743499	8.50×10^{-11}	2.37×10^{-24}	2.985	0.615	0.12
11	190023.4–581620	31.4248595701	5.07×10^{-13}	1.80×10^{-23}	1.906	0.412	5.16
12	220724.6–165822	39.7247751375	6.25×10^{-9}	2.66×10^{-25}	1.527	–0.068	2.79

Base frequencies are solar system barycentered at Jul 07, 2009 21:00:00 UTC (the start of S6). The first derivatives \dot{f} were constant, i.e. the injections did not include second derivatives. The inclination angle ι , polarization angle ψ , and signal phase offset ϕ_0 were not used in this work. They, and the detailed waveforms, are explained in detail in Jaranowski et al. (1998).

With these searches we were able to detect all ten hardware injections above the “further look” threshold (95% confidence in Gaussian noise). Since Pulsar 0 was just barely above threshold in the first search, we made a first follow-up by doubling the integration time to 20 days to verify that $2\mathcal{F}$ doubled, similar to what would have been done in the early stages of following up a plausible non-injected candidate. The loudest injections (Pulsar 3 and Pulsar 8) triggered the Fscan veto, which had to be switched off to complete this exercise. Although this might cause concerns about the safety of the veto, these injections are unreasonably loud, with $2\mathcal{F} \approx 2 \times 10^4$. Real signals that loud would have been detected in earlier LIGO data runs. Also, very few frequency bands triggered an Fscan veto in both detectors, and we checked that (other than the loud hardware injections) these bands corresponded to known instrumental artifacts. By contrast, Pulsar 4 had $2\mathcal{F} \approx 2 \times 10^4$ and was not Fscan-vetoed, apparently because of its large $|\dot{f}| > 2.5 \times 10^{-8}$ Hz/s spreading the power over several SFT bins.

The recovered parameters of the hardware injections were typically off by the amount expected from template parameter discretization and the fact that the injections did not include a second spin-down parameter while the search templates did. In a real potential detection scenario, candidates would have been followed up in a more sophisticated way, such as a hierarchical search or the gridless method of Shaltev & Prix (2013).

REFERENCES

- Aasi, J., et al. 2013a, *Phys. Rev. D*, 88, 102002
—, 2013b, *Phys. Rev. D*, 87, 042001
—, 2014a, *Class. Quantum Grav.*, 31, 085014
—, 2014b, *Phys. Rev. D*, 90, 062010
—, 2014c, *ApJ*, 785, 119
—, 2014d, *Class. Quantum Grav.*, 31, 165014
—, 2015a, *Class. Quant. Grav.*, 32, 074001
—, 2015b, *Class. Quant. Grav.*, 32, 115012
—, 2015c, *Phys. Rev. D*, 91, 062008
Abadie, J., et al. 2010, *ApJ*, 722, 1504
—, 2011a, *ApJ*, 737, 93
—, 2011b, *Phys. Rev. Lett.*, 107, 261102
—, 2012, *Phys. Rev. D*, 85, 022001
Abbott, B., et al. 2004, *Phys. Rev. D*, 69, 082004
—, 2005a, *Phys. Rev. D*, 72, 102004
—, 2005b, *Phys. Rev. Lett.*, 94, 181103
—, 2007a, *Phys. Rev. D*, 76, 082001
—, 2007b, *Phys. Rev. D*, 76, 082003
—, 2007c, *Phys. Rev. D*, 76, 042001
—, 2008a, *Phys. Rev. D*, 77, 022001
—, 2008b, *ApJ*, 683, L45
—, 2009a, *Phys. Rev. D*, 79, 022001
Abbott, B. P., et al. 2009b, *Phys. Rev. Lett.*, 102, 111102
—, 2009c, *Phys. Rev. D*, 80, 042003
—, 2010, *ApJ*, 713, 671
Allen, G., Chow, K., DeLaney, T., et al. 2015, *Astrophys. J.*, 798, 82
Andersson, N. 1998, *Astrophys. J.*, 502, 708
Bartos, I., et al. 2011, Frequency domain calibration error budget for LIGO in S6, LIGO Technical Document T1100071, <https://dcc.ligo.org>
Bildsten, L. 1998, *ApJ*, 501, L89
Bondaescu, R., Teukolsky, S. A., & Wasserman, I. 2009, *Phys. Rev. D*, 79, 104003
Brady, P. R., Creighton, T., Cutler, C., & Schutz, B. F. 1998, *Phys. Rev. D*, 57, 2101
Cassam-Chenaï, G., Decourchelle, A., Ballet, J., et al. 2004, *A&A*, 427, 199
Ciolfi, R., & Rezzolla, L. 2013, *MNRAS*, 435, L43
Cutler, C., & Schutz, B. F. 2005, *Phys. Rev. D*, 72, 063006
Fesen, R. A., & Kirshner, R. P. 1980, *ApJ*, 242, 1023
Fesen, R. A., Kremer, R., Patnaude, D., & Milisavljevic, D. 2012, *AJ*, 143, 27
Fesen, R. A., et al. 2006, *ApJ*, 645, 283
Foster, T., & Routledge, D. 2003, *ApJ*, 598, 1005
Gaensler, B. M., Tanna, A., Slane, P. O., et al. 2008, *ApJ*, 680, L37
Gotthelf, E. V., & Halpern, J. P. 2008, in *American Institute of Physics Conference Series*, Vol. 983, 40 Years of Pulsars: Millisecond Pulsars, Magnetars and More, ed. C. Bassa, Z. Wang, A. Cumming, & V. M. Kaspi, 320–324
Green, D. 2014, *Bull. Astron. Soc. India*, 42, 47
Green, D. A. 2009, *Bull. Astron. Soc. India*, 37, 45
Harrus, I. M., Slane, P. O., Hughes, J. P., & Plucinsky, P. P. 2004, *ApJ*, 603, 152
Harry, G. M. 2010, *Class. Quantum Grav.*, 27, 084006
Idrisy, A., Owen, B. J., & Jones, D. I. 2015, *Phys. Rev. D*, 91, 024001
Iyudin, A. F., Schönfelder, V., Bennett, K., et al. 1998, *Nature*, 396, 142
Jaranowski, P., Krolak, A., & Schutz, B. F. 1998, *Phys. Rev. D*, 58, 063001
Jiang, B., Chen, Y., & Wang, Q. D. 2007, *ApJ*, 670, 1142
Johnson-McDaniel, N. K. 2013, *Phys. Rev. D*, 88, 044016
Johnson-McDaniel, N. K., & Owen, B. J. 2013, *Phys. Rev. D*, 88, 044004
Katsuda, S., Tsunemi, H., & Mori, K. 2008, *ApJ*, 678, L35
Keitel, D., Prix, R., Papa, M. A., Leaci, P., & Siddiqi, M. 2014, *Phys. Rev. D*, 89, 064023
Knispel, B., & Allen, B. 2008, *Phys. Rev. D*, 78, 044031
Lindblom, L., Owen, B. J., & Morsink, S. M. 1998, *Phys. Rev. Lett.*, 80, 4843
Lovchinsky, I., Slane, P., Gaensler, B. M., et al. 2011, *ApJ*, 731, 70
Mastrano, A., Melatos, A., Reisenegger, A., & Akgün, T. 2011, *MNRAS*, 417, 2288
Mignani, R. P., Zaggia, S., de Luca, A., et al. 2008, *A&A*, 484, 457

- Moffett, D., Gaensler, B., & Green, A. 2001, in AIP Conf. Proc., Vol. 565, Young Supernova Remnants: Eleventh Astrophysics Conference, ed. S. S. Holt & U. Hwang (Melville, NY: AIP), 333–336
- Olbert, C. M., Clearfield, C. R., Williams, N. E., Keohane, J. W., & Frail, D. A. 2001, *ApJ*, 554, L205
- Owen, B. J. 1996, *Phys. Rev. D*, 53, 6749
- . 2005, *Phys. Rev. Lett.*, 95, 211101
- . 2009, *Class. Quantum Grav.*, 26, 204014
- . 2010, *Phys. Rev. D*, 82, 104002
- Papaloizou, J., & Pringle, J. E. 1978, *MNRAS*, 184, 501
- Pavlov, G. G., Sanwal, D., Kızıltan, B., & Garmire, G. P. 2001, *ApJ*, 559, L131
- Petre, R., Szymkowiak, A. E., Seward, F. D., & Willingale, R. 1988, *ApJ*, 335, 215
- Prix, R. 2009, The \mathcal{F} -statistic and its implementation in `ComputeFStatistic_v2`, LIGO Technical Document T0900149, <https://dcc.ligo.org>
- Prix, R., & Krishnan, B. 2009, *Class. Quantum Grav.*, 26, 204013
- Reed, J. E., Hester, J. J., Fabian, A. C., & Winkler, P. F. 1995, *ApJ*, 440, 706
- Reich, W., Fuerst, E., Haslam, C. G. T., Steffen, P., & Reif, K. 1984, *A&AS*, 58, 197
- Reynolds, S. P., Borkowski, K. J., Green, D. A., et al. 2008, *ApJ*, 680, L41
- Sammut, L., Messenger, C., Melatos, A., & Owen, B. 2014, *Phys. Rev. D*, 89, 043001
- Shaltev, M., & Prix, R. 2013, *Phys. Rev. D*, 87, 084057
- Shklovskii, I. S. 1969, *AZh*, 46, 715
- Slane, P., Gaensler, B. M., Dame, T. M., et al. 1999, *ApJ*, 525, 357
- Slane, P., Hughes, J. P., Temim, T., et al. 2012, *ApJ*, 749, 131
- Tananbaum, H. 1999, *IAU Circ.*, 7246, 1
- Tüllmann, R., Plucinsky, P. P., Gaetz, T. J., et al. 2010, *ApJ*, 720, 848
- Wang, Z. R., Qu, Q., & Chen, Y. 1997, *A&A*, 318, L59
- Wette, K. 2012, *Phys. Rev. D*, 85, 042003
- Wette, K., et al. 2008, *Class. Quantum Grav.*, 25, 235011
- Whitbeck, D. M. 2006, PhD thesis, The Pennsylvania State University